Ref.

NBS TECHNICAL NOTE 592

TED STATES
TMENT OF
MMERCE
ICATION

Methods of Measurement for Semiconductor Materials, Process Control, and Devices

Quarterly Report

October 1 to December 31, 1970

U.S.
RTMENT
OF
MMERCE
National
Bureau
of
Standards

.3
?2.
!
1!.

NATIONAL BUREAU OF STANDARDS

The National Bureau of Standards[1] was established by an act of Congress March 3, 1901. The Bureau's overall goal is to strengthen and advance the Nation's science and technology and facilitate their effective application for public benefit. To this end, the Bureau conducts research and provides: (1) a basis for the Nation's physical measurement system, (2) scientific and technological services for industry and government, (3) a technical basis for equity in trade, and (4) technical services to promote public safety. The Bureau consists of the Institute for Basic Standards, the Institute for Materials Research, the Institute for Applied Technology, the Center for Computer Sciences and Technology, and the Office for Information Programs.

THE INSTITUTE FOR BASIC STANDARDS provides the central basis within the United States of a complete and consistent system of physical measurement; coordinates that system with measurement systems of other nations; and furnishes essential services leading to accurate and uniform physical measurements throughout the Nation's scientific community, industry, and commerce. The Institute consists of a Center for Radiation Research, an Office of Measurement Services and the following divisions:

Applied Mathematics—Electricity—Heat—Mechanics—Optical Physics—Linac Radiation[2]—Nuclear Radiation[2]—Applied Radiation[2]—Quantum Electronics[3]—Electromagnetics[3]—Time and Frequency[3]—Laboratory Astrophysics[3]—Cryogenics[3].

THE INSTITUTE FOR MATERIALS RESEARCH conducts materials research leading to improved methods of measurement, standards, and data on the properties of well-characterized materials needed by industry, commerce, educational institutions, and Government; provides advisory and research services to other Government agencies; and develops, produces, and distributes standard reference materials. The Institute consists of the Office of Standard Reference Materials and the following divisions:

Analytical Chemistry—Polymers—Metallurgy—Inorganic Materials—Reactor Radiation—Physical Chemistry.

THE INSTITUTE FOR APPLIED TECHNOLOGY provides technical services to promote the use of available technology and to facilitate technological innovation in industry and Government; cooperates with public and private organizations leading to the development of technological standards (including mandatory safety standards), codes and methods of test; and provides technical advice and services to Government agencies upon request. The Institute also monitors NBS engineering standards activities and provides liaison between NBS and national and international engineering standards bodies. The Institute consists of the following technical divisions and offices:

Engineering Standards Services—Weights and Measures—Flammable Fabrics—Invention and Innovation—Vehicle Systems Research—Product Evaluation Technology—Building Research—Electronic Technology—Technical Analysis—Measurement Engineering.

THE CENTER FOR COMPUTER SCIENCES AND TECHNOLOGY conducts research and provides technical services designed to aid Government agencies in improving cost effectiveness in the conduct of their programs through the selection, acquisition, and effective utilization of automatic data processing equipment; and serves as the principal focus within the executive branch for the development of Federal standards for automatic data processing equipment, techniques, and computer languages. The Center consists of the following offices and divisions:

Information Processing Standards—Computer Information—Computer Services—Systems Development—Information Processing Technology.

THE OFFICE FOR INFORMATION PROGRAMS promotes optimum dissemination and accessibility of scientific information generated within NBS and other agencies of the Federal Government; promotes the development of the National Standard Reference Data System and a system of information analysis centers dealing with the broader aspects of the National Measurement System; provides appropriate services to ensure that the NBS staff has optimum accessibility to the scientific information of the world, and directs the public information activities of the Bureau. The Office consists of the following organizational units:

Office of Standard Reference Data—Office of Technical Information and Publications—Library—Office of Public Information—Office of International Relations.

[1] Headquarters and Laboratories at Gaithersburg, Maryland, unless otherwise noted; mailing address Washington, D.C. 20234.
[2] Part of the Center for Radiation Research.
[3] Located at Boulder, Colorado 80302.

L BUREAU OF STANDARDS

UNITED STATES DEPARTMENT OF COMMERCE
Maurice H. Stans, Secretary
NATIONAL BUREAU OF STANDARDS • Lewis M. Branscomb, Director

NBS TECHNICAL NOTE 592

ISSUED AUGUST 1971

Nat. Bur. Stand. (U.S.), Tech. Note 592, 72 pages (Aug. 1971)
CODEN: NBTNA

Methods of Measurement for Semiconductor Materials, Process Control, and Devices

Quarterly Report

October 1 to December 31, 1970

Edited by W. Murray Bullis

Electronic Technology Division
Institute for Applied Technology
National Bureau of Standards
Washington, D.C. 20234

Jointly Supported by the National Bureau of Standards, the Defense Atomic Support Agency, the U.S. Navy Strategic Systems Project Office, the U.S. Navy Electronic Systems Command, the Atomic Energy Commission, and the National Aeronautics and Space Administration

NBS Technical Notes are designed to supplement the Bureau's regular publications program. They provide a means for making available scientific data that are of transient or limited interest. Technical Notes may be listed or referred to in the open literature.

For sale by the Superintendent of Documents, U.S. Government Printing Office, Washington, D.C., 20402.
(Order by SD Catalog No. C 13.46:592). Price 50 cents.
Stock Number – C13.46:592

CONTENTS

PAGE

Foreword vi

1. Introduction 1

2. Highlights 3

3. Methods of Measurement for Semiconductor Materials

3.1. Resistivity 8

3.2. Carrier Lifetime 14

3.3. Inhomogeneities 17

3.4. Gold-Doped Silicon 18

3.5. Specification of Germanium 21

3.6. References 27

4. Methods of Measurement for Semiconductor Process Control

4.1. Metallization Evaluation 29

4.2. Die Attachment Evaluation 32

4.3. Wire Bond Evaluation 34

4.4. Processing Facility 45

4.5. References 48

5. Methods of Measurement for Semiconductor Devices

5.1. Thermal Properties of Devices 49

5.2. Thermographic Measurements 56

5.3. Microwave Device Measurements 57

5.4. Carrier Transport in Junction Devices 59

5.5. Silicon Nuclear Radiation Detectors 60

5.6. References 62

Appendix A. Joint Program Staff 63

Appendix B. Committee Activities 64

Appendix C. Solid-State Technology & Fabrication Services 66

Appendix D. Joint Program Publications 67

LIST OF FIGURES

PAGE

1. Gold concentration as determined by neutron activation analysis as a function of diffusion time for 10- and 20-Ω·cm, boron-doped, gold-diffused, silicon wafers 20

2. Oxygen concentration, N_O, obtained from lithium precipitation (●) and infrared absorption measurements (○) plotted against N_O obtained from lithium mobility measurements 23

3. Infrared response (IRR) spectra obtained using a 3-mm thick germanium filter 24

4. IRR spectra in the incident photon energy range of 0.30 to 0.70 eV obtained using a 1-mm thick germanium filter 26

5. Transient thermal response curve for a typical mesa diode on a 0.95-mm square chip mounted on a TO-5 header 33

6. Laser system set-up for calibrating ultrasonic bonding tool vibration amplitude 38

7. A comparison between the output of a microphone and a laser interferometer simultaneously monitoring the same loose bonding tool 38

8. Schematic representation of mixer system for monitoring ultrasonic bond formation 40

9. Measurement of the self-induced vibrations of a bonding machine 42

10. Improved electromagnetic displacement sensor and wire indentation tester 44

11. Electron-beam evaporation system 45

12. Schematic representation of silicon dioxide vapor deposition system 46

13. Apparatus for measuring dynamics of photoresist spinners . . . 46

14. Base current as a function of collector-emitter voltage for a 35-W, triple-diffused, silicon transistor 50

15. Base current as a function of collector-emitter voltage for a 20-W, triple-diffused, silicon power transistor 51

16. Data used to calculate the thermal resistance of a 35-W, triple-diffused, silicon transistor as a function of applied power 52

17. Common-emitter current gain, h_{FE}, and thermal resistance, R_{Θ}, of a 35-W, triple-duffused, silicon transistor as a function of applied power, P 54

18. Thermal resistance, R_{Θ}, as a function of case temperature, T_C, for a 35-W, epitaxial-diffused, silicon transistor 54

19. Spatial resolution of fiber optic probes compared by scanning a black-white boundary on a Microcopy Resolution Test Chart and recording the changes in photometer output 56

LIST OF TABLES

1. Thickness Correction Factor, $F(w/\bar{S})$ 11

2. Results of Scratch Tests on a 1.0-μm Thick Aluminum Film with an 18-μm Diamond Stylus 31

FOREWORD

The Joint Program on Methods of Measurement for Semiconductor Materials, Process Control, and Devices was undertaken in 1968 to focus NBS efforts to enhance the performance, interchangeability, and reliability of discrete semiconductor devices and integrated circuits through improvements in methods of measurement for use in specifying materials and devices and in control of device fabrication processes. These improvements are intended to lead to a set of measurement methods which have been carefully evaluated for technical adequacy, which are acceptable to both users and suppliers, which can provide a common basis for the purchase specifications of government agencies, and which will lead to greater economy in government procurement. In addition, such methods will provide a basis for controlled improvements in essential device characteristics, such as uniformity of response to radiation effects.

The Program is supported by the National Bureau of Standards,[†] the Defense Atomic Support Agency,[*] the U. S. Navy Strategic Systems Project Office,[§] the U. S. Navy Electronics Systems Command,[+] the Atomic Energy Commission,[#] and the National Aeronautics and Space Administration.[×] There is not a one-to-one correspondence between the tasks described in this report and the projects by which the Program is supported. Although all sponsors subscribe to the need for the entire basic program for improvement of measurement methods for semiconductor materials, process control, and devices, the concern of certain sponsors with specific parts of the Program is reflected in planning and conduct of the work.

---

† Through Research and Technical Services Projects 4251120, 4251123, 4251126, 4252114, 4252119, 4252128, 4254111, 4254112, and 4254115.

* Through Order EA071-801. (NBS Project 4259522).

§ Administered by U. S. Naval Ammunition Depot, Crane, Indiana through Project Orders PO-1-0030 and PO-1-0041. (NBS Project 4259533)

+ Through Project Order PO-1-1057. (NBS Project 4252534)

Division of Biology and Medicine. (NBS Project 4259425)

× Through Orders S-70003-G, Goddard Space Flight Center, and H-76553A, Marshall Space Flight Center. (NBS Projects 4254429 and 4251449)

METHODS OF MEASUREMENT FOR SEMICONDUCTOR MATERIALS, PROCESS CONTROL, AND DEVICES

Quarterly Report
October 1 to December 31, 1970

ABSTRACT

This quarterly progress report, tenth of a series, describes NBS activities directed toward the development of methods of measurement for semiconductor materials, process control, and devices. Significant accomplishments during this reporting period include successful application of the surface photovoltage technique, a non-contacting method, to the measurement of carrier diffusion length in silicon epitaxial layers and development of a novel, but simple, method for measurement of acceleration and terminal angular velocity of a photoresist spinner. Work is continuing on measurement of resistivity, carrier lifetime, and electrical inhomogeneities in semiconductor crystals; specification of germanium for gamma-ray detectors; evaluation of wire bonds, metallization adhesion, and die attachment; measurement of thermal properties of semiconductor devices, transit-time and related carrier transport properties in junction devices, and electrical properties of microwave devices; and characterization of silicon nuclear radiation detectors. Supplementary data concerning staff, standards committee activities, technical services, and publications are included as appendixes.

Key Words: Alpha-particle detectors; aluminum wire; base transit time; carrier lifetime; die attachment; electrical properties; epitaxial silicon; gamma-ray detectors; germanium; gold-doped silicon; metallization; methods of measurement; microelectronics; microwave devices; nuclear radiation detectors; probe techniques (a-c); resistivity; semiconductor devices; semiconductor materials; semiconductor process control; silicon; thermal resistance; thermographic measurements; ultrasonic bonder; wire bonds.

1. INTRODUCTION

This is the tenth quarterly report to the sponsors of the Joint Program on Methods of Measurement for Semiconductor Materials, Process Control, and Devices. It summarizes work on a wide variety of measurement methods that are being studied at the National Bureau of Standards. Since the Program is a continuing one, the results and conclusions reported here are subject to modification and refinement.

Fourteen tasks, each directed toward a particular material or device property or measurement technique, have been identified as parts of the Program. The report is subdivided according to these tasks. Highlights of activity during the quarter are given in Section 2. Section 3 deals with tasks on methods of measurement for materials; Section 4, with those on methods of measurement for process control; and Section 5, with those on methods of measurement for devices. References for each section are listed in a separate subsection at the end of that section.

An important part of the work which frequently goes beyond the task structure is participation in the activities of various technical standardizing committees. The list of personnel involved with this work given in Appendix B suggests the extent of this participation. Additional details of current efforts in this area are given in Section 2.

The report of each task includes the long-term objective, a narrative description of progress made during this reporting period, and a listing of plans for the immediate future. Additional information concerning the material reported may be obtained directly from individual staff members connected with the task as indicated throughout the report. The organization of the Joint Program staff and telephone numbers are listed in Appendix A.

Background material on the Program and individual tasks may be found in earlier reports in this series as listed in Appendix D. From time to time, publications that describe some aspect of the program in greater detail are prepared. Current publications are also listed in Appendix D.

2. HIGHLIGHTS

Highlights of the technical activity during this reporting period are presented in this section; details are given in subsequent sections of the report.

Resistivity — The study of current and probe force dependence of resistivity as measured by the four-probe method was interrupted while several changes in the experimental procedure were evaluated. It was observed that the sensitivity of the four-probe apparatus to mechanical vibrations is lowest when the line of probe points is perpendicular to the supporting boom. A simplified computation procedure for the correction factor appropriate to four-probe resistivity measurements on wafers with finite thickness was developed in a form suitable for use on a programmable desk calculator. Investigation of temperature coefficient data for silicon showed that the published coefficients can be used to correct resistivity measurements to any referenced temperature in the range 20 to 25°C with the same limitations that apply to correction to the standard reference temperature, 23°C. Development work on procedures for examining probe damage in silicon with the scanning electron microscope is continuing in connection with work on the spreading resistance method. A change in the diffusion procedure has enabled diodes with more abrupt junctions and higher breakdown voltages to be fabricated. Although preliminary capacitance-voltage measurements were made on some of these diodes, the analysis was not completed.

Carrier Lifetime — Increased emphasis was placed on the study of the photoconductive decay method for measuring bulk carrier lifetime. The dependence of the measured value of lifetime on signal level, applied electric field, chopped-light turn-off time, and series resistance was established. An experiment to determine the relative single laboratory precision of the time-mark method and the null method for measuring photoconductive decay time was begun. The measuring circuit for the metal-oxide-semiconductor capacitance method for measuring carrier lifetime in epitaxial layers was calibrated, and initial measurements were carried out.

Previously observed variability in the measurement of the surface photovoltage was greatly reduced by shielding the specimen and thermopile from ambient room light. This new, non-contacting technique was successfully applied to the measurement of carrier diffusion length in silicon epitaxial layers.

Inhomogeneities — Correlation studies between photovoltaic, four-probe, and two-probe resistivity profiles were continued. An investigation into the various factors which may affect precision and accuracy of the profiles determined by each of the three measurement methods was initiated.

Gold-Doped Silicon — The effect of gold accumulated at the rim of gold-diffused wafers on the determination of concentration by neutron activation analysis was established. Rim portions of wafers diffused at temperatures below 1250°C showed erroneously high concentrations. Boron-doped silicon wafers diffused in an oxygen atmosphere showed higher concentrations of gold than similar wafers diffused in an argon atmosphere. Several relatively high resistivity *p*-type specimens showed the same unexplained decrease in resistivity with increasing gold concentration at high gold concentrations that had been observed earlier elsewhere.

Specification of Germanium — Analysis of the data obtained in the comparison study of the lithium mobility and the lithium precipitation methods for determining oxygen concentration in germanium has been completed. The improved infrared response technique was used to examine several additional lithium-drifted germanium diodes. The results show that this technique is capable of detecting impurities such as copper and identifying them by means of their observed energy levels. It can detect such impurities at concentrations below 10^{14} cm^{-3} and appears to be more sensitive than other methods which have been used.

Metallization Evaluation — Study of the scratch test was extended to the case of thicker aluminum films deposited on quartz substrates. Some differences in failure characteristics were observed, but they could not be attributed unambiguously to the change in thickness. Preliminary study of methods for detecting threshold adhesion failure in the aluminum-silicon dioxide-silicon system was begun.

Die Attachment Evaluation — Increased emphasis was placed on this area during this reporting period. Detailed studies of the reproducibility of the thermal response curve for batches of diodes were initiated. The reproducibility achieved in the first experiments suggests that the measurement of thermal response after a heating power pulse a few milliseconds long is a sensitive indicator of die attachment quality. Development of procedures for bonding diodes with voids of controlled area and location in the die attachment continued.

Wire Bond Evaluation — Study of the effect of pull rate on the pull test revealed that, when the failure occurred at the heel of the first bond, pulling at a rate equivalent to the "jerk" test used by some device manufacturers gives results statistically equivalent to those obtained by pulling at the much slower rates previously studied. The importance of specifying all details of the pull test including the wire bond failure mode has become apparent.

Tests carried out to simulate the high temperature environment encountered by bonds during glass sealing operations for ceramic packages showed that the reduction in pull strength can be accounted for principally by the reduction in wire tensile strength caused by the high temperature anneal.

Improvements in the laser mount for interferometry measurements were made to increase the ease of optical alignment and use of the interferometer on bonding machines. The length of the laser was increased in order to limit all emission to the TEM_{00} mode.

New experiments directed toward development of measurement methods applicable to in-process bond quality determination were started. The initial effort consisted of electronically mixing the 60-kHz output from the capacitor microphone directed at the bonding tool with a local oscillator. Preliminary results showed that the bonding process can be heard through an audio speaker and recorded on magnetic tape. Harmonics of the tool motion can be individually treated in the same manner. It is expected that the harmonic characteristics can be correlated with bond quality.

An improved electromagnetic displacement sensor was designed and built for the wire indentation tester which is nearing completion.

Processing Facility — Installation of a 10-kW electron beam evaporation system for the deposition of aluminum was completed. A system was built to deposit vitreous silicon dioxide films from silane so that silicon dioxide layers may be produced at low temperatures.

A novel, but simple, method was developed for the measurement of the acceleration and terminal angular velocity of a photoresist spinner.

Thermal Properties of Devices — Work continued on the preparation of a suitable measurement procedure and data collection format for the preliminary thermal resistance round robin being conducted by JEDEC Committee JC-25 on Power Transistors.

It was found that the increase in the thermal resistance which is sometimes observed as case temperature increases can be related to the increase in thermal resistivity of the silicon chip with temperature. The results of a study undertaken to determine the effect of variations in device case temperature on the voltage at which a hot spot was formed suggest that hot-spot formation is governed by the magnitude of a localized temperature increase in the transistor rather than by the absolute temperature of the chip. This result appears to be consistent with a previously proposed model for thermal hysteresis.

Microwave Device Measurements — The audio i-f portion of the X-band mixer diode measurement system was built and tested. A measurement technique was developed to enable the mixer i-f resistance to be read directly from a calibrated precision decade resistance box. A feedback loop was constructed to improve the amplitude stability of the local oscillator in the r-f portion of the X-band system.

Carrier Transport in Junction Devices — Construction, initial testing, and adjustment of the Sandia-type delay-time bridge were completed. A preliminary analysis of the bridge showed that the delay time read from the line stretchers can be made to be independent of mismatch between the line stretchers and the transistor being measured. Field and literature surveys of both delay time measurement and probing techniques were continued.

Silicon Nuclear Radiation Detectors — Preflight bench-testing of lithium-drifted silicon radiation detectors continued. Initial experiments were conducted in the ambient exposure test program to determine the effects of hazardous ambients on the performance characteristics of lithium-drifted and surface-barrier silicon detectors. Eight lithium-drifted silicon detectors were acquired for radiation damage experiments.

Standardization Activities — Many of the standardization activities undertaken by program staff members are broader than the technical tasks described in the following sections. These activities involve both coordination of efforts which may encompass a variety of tasks and participation in areas where no direct technical effort is presently underway.

W. M. Bullis and D. E. Sawyer attended an intersociety meeting on Need for Standards in Radiation Effects on Electronic Parts, Materials, and Devices organized by R. S. Shane of American Society for Testing and Materials (ASTM) Committee E-10 on Radioisotopes and Radiation Effects in October. The Institute of Electrical and Electronics Engineers (IEEE), Society of Automotive Engineers (SAE), Americal Institute of Aeronautics and Astronautics (AIAA), American Nuclear Society (ANS), and ASTM were represented in addition to various government agencies. At this meeting the various requirements for standard test methods, nomenclature, formats, and specifications in this field were discussed and various areas were referred to the groups represented for appropriate action. The development of test methods appropriate to electronic materials and devices was referred to both IEEE and ASTM. Program staff members are active participants in all appropriate groups in these societies.

W. M. Bullis presented an invited discussion of standardization efforts in the integrated circuit field at the fall meeting of SAE Committee H on Electronic Materials and Processes. This committee is presently undergoing reorganization in an effort to focus appropriate attention on the development of specifications of parts and materials for integrated circuits.

At the invitation of the chairman, J. C. French attended a meeting of SAE Subcommittee A-2N on Radiation Hardening and Nuclear Survivability. He was asked to provide continuing liaison to the subcommittee in regard to test method development in ASTM Committee F-1.

Mrs. K. O. Leedy organized the Washington Area Scanning Electron Microscopists in order to provide a medium of exchange for local workers in this important diagnostic field. The organization has over 80 members and conducts monthly meetings arranged around a technical presentation in the field.

The reorganization of the Electronic Industries Association Committees on Semiconductor Devices (JEDEC) and Microelectronics (MED) into the Solid State Division has caused some rearrangement of activity by Program staff members. Participation in the new committee structure is indicated in Appendix B. F. F. Oettinger has been requested to chair a Task Group on Microelectronics Thermal Considerations of Subcommittee 3 on Microelectronic Devices of Committee JC-11 on Mechanical Standardization. Other activities directly related to thermal resistance measurements are reported in Section 4.1.

Although there was no meeting of ASTM Committee F-1 during this quarter, considerable round robin and editorial review activity continued in a variety of areas.

3. METHODS OF MEASUREMENT FOR SEMICONDUCTOR MATERIALS

3.1. RESISTIVITY

Objective: To develop methods, suitable for use throughout the electronics industry, for measuring resistivity of bulk, epitaxial, and diffused silicon wafers.

Progress: Data collection activity on the study of current and probe force dependence of resistivity as measured by the four-probe method was interrupted while several changes in the experimental procedure were evaluated. A simplified computation procedure for the correction factor for finite wafer thickness was developed in a form suitable for use on a programmable desk calculator. Investigation of temperature coefficient data for silicon showed that the published coefficients can be used to correct resistivity measurements to any reference temperature in the range 20 to 25°C from a measurement temperature up to 5°C different from the reference temperature. Work on the spreading resistance method has been concentrated on development of procedures for examining probe damage in silicon with the scanning electron microscope. Diodes with more abrupt junctions and higher breakdown voltages have been fabricated and studied by the capacitance-voltage method.

Four-Probe Method — The study of current and probe force dependence of resistivity as measured by the four-probe method on mechanically polished slices is being delayed pending investigation of certain changes in experimental procedure. The object of this study has been to distinguish changes in measured resistivity with change in probe force, current level, or surface preparation at or near the one-percent level. Difficulties in the statistical analysis of measurements previously made on wafers with lapped surfaces could be attributed to the fact that for a number of measurements the average resistivity or measured precision was too far outside the consensus for the wafer. A plot of average resistivity against standard deviation was made for all data taken on each wafer. The data for each wafer which included all combinations of current level and probe loading used in the test (NBS Tech. Note 555, pp. 6-7) tended to cluster except for a few scattered points. In general, data taken at the intermediate probe load of 50 g produced the largest number of data points lying outside the cluster. The cause of this observation has not yet been identified.

Heretofore measurements at each probe loading have been made with a different four-probe head. Because the probe point quality might vary from head to head, this has introduced an extra variable into the procedure. A short investigation showed that probe springs can be preset for a given probe head and reproducibly inserted when needed if care is taken to lock the adjustment screws in place and if small shims are added to the probe head so that each spring block can be repeatably mounted at

the same height within the probe head. With the use of these procedures the same probe head and probe point set can be used for all future measurements.

Microscopic examination of polished wafers after a series of measurements indicated a considerably larger probability of placing the probe points in previously damaged spots than had been anticipated. Earlier work on lapped surfaces had shown an increased scatter of data when measurements are taken in previously damaged locations. These two observations suggest that data should be taken at all current values before changing wafer orientation rather than at a single current value for all wafer orientations as has been done so far. Several specimens are being investigated to determine the effect on precision if the data-taking sequence is modified in this way. (F. H. Brewer and D. R. Ricks)

During the course of the investigation, some unreasonably random data were encountered on a 100-Ω·cm *p*-type slice. A subsequent check disclosed that the four-probe apparatus is quite sensitive to vibrations, both transmitted through the laboratory and air-borne, such as voice. This microphonic signal is directly proportional to the current level used for measurement of any one wafer; for equal current levels on different wafers it is proportional to the power supply compliance voltage. This microphonic signal was observed on all wafers with resistivity above 0.01 Ω·cm. It is believed that vibration results in oscillation of the probe point and of its associated contact resistance to the wafer and that the output of the power supply then oscillates as it tries to maintain constant current. Indeed, current oscillations were measured as a result of these fluctuations. Spurious signals as large as 5 V could be induced across the current probe points by footfalls near the equipment bench when operating at a 150-V compliance voltage on 100-Ω·cm material. This produced as much as 60 mV of spurious normal mode signal with a distorted, modulated 60-Hz wave form at the voltage measuring probes. An erroneous measurement of slice resistivity may result from such a signal since it may not be fully rejected by the digital voltmeter. The use of acoustic padding under the probe stand and a vacuum chuck to hold the wafer reduced the "noise" by about 40 percent. It was also observed that changing the orientation of the probe head in its clamp could also result in about a 50-percent change in the susceptibility of the probe to vibrations. An orientation with the line of probe points transverse to the axis of the supporting boom was found to be preferable. (J. R. Ehrstein)

Correction Factor for Finite Thickness — The resistivity ρ of a thin sheet of material of thickness w as measured by a collinear four-probe array of spacing $\bar{S}$ is

$$\rho = \frac{V}{I} \cdot w \cdot \frac{\pi}{\ln 2} \cdot F(w/\bar{S}) \qquad (1)$$

where I is the current passing through the outer probes and V is the potential difference between the inner probes. The correction factor $F(w/\bar{S})$ has been calculated by Smits [1] using methods developed by Uhlir [2]. If the sheet is surrounded by insulating media

$$F(w/\bar{S}) = 2 \ln 2 \cdot \frac{\bar{S}}{w} \cdot \frac{1}{G_7(w/\bar{S})} \tag{2}$$

where [3]

$$G_7(w/\bar{S}) = 1 + 2 \sum_{n=1}^{\infty} \{[(1/4) + (nw/\bar{S})^2]^{-\frac{1}{2}} - [1 + (nw/\bar{S})^2]^{-\frac{1}{2}}\}. \tag{3}$$

For a thin wafer, the summation in $G_7(w/\bar{S})$ converges very slowly; great care must be taken and multiple precision arithmetic must be used to prevent a significant accumulation of round-off errors.

The problems of subtracting two nearly equal terms can be avoided by expanding each of the terms in a binomial series and performing the subtraction before computing the terms. In this case

$$G_7(\frac{w}{\bar{S}}) = 1 + \sum_{n=1}^{\infty} [\frac{3}{4} (\frac{\bar{S}}{nw})^3 - \frac{45}{64} (\frac{\bar{S}}{nw})^5 + \frac{315}{512} (\frac{\bar{S}}{nw})^7 - \cdots]. \tag{4}$$

Convergence here requires that $nw > \bar{S}$; if $nw < 2\bar{S}$, additional terms in the binomial expansion are required for satisfactory precision.

In calculating the functions from which he computed his correction factors, Uhlir [2] suggested switching from one series to the other at an appropriate value for n. This technique is satisfactory in the present case if the switch is made after M terms where M is the smallest value of n for which the inequality $n > 2\bar{S}/w$ applies. The series (4) is truncated after N terms where the Nth term is required to have a value less than a specified residual. Then eq (3) becomes:

$$G_7(\frac{w}{\bar{S}}) = 1 + 2 \sum_{n=1}^{M} \{[\frac{1}{4} + (\frac{nw}{\bar{S}})^2]^{-\frac{1}{2}} - [1 + (\frac{nw}{\bar{S}})^2]^{-\frac{1}{2}}\}$$
$$+ \sum_{n=M+1}^{N} [\frac{3}{4} (\frac{\bar{S}}{nw})^3 - \frac{45}{64} (\frac{\bar{S}}{nw})^5 + \frac{315}{512} (\frac{\bar{S}}{nw})^7]. \tag{5}$$

The computation may be carried out easily on a programmable desk calculator or larger computer. The results are given in table 1. The values quoted by Smits [1] are listed in column 2 while interpolated values [4] for even tenths are listed in column 3. Results of the present

calculation agree to within 1 part in 10^4 with those of Smits except for $w/\bar{S} = 1$. In this calculation the Nth term was required to be smaller than 10^{-5}.

Table 1 — Thickness Correction Factor, $F(w/\bar{S})$

$w/\bar{S}$	Smits' [1]	F84 [4]	Present Calculation		
	$F(w/\bar{S})$	$F(w/\bar{S})$	M	N	$F(w/\bar{S})$
0.1	1.0000		21	422	1.0000
0.2	1.0000		11	211	1.0001
0.4	0.9995		6	106	0.9996
0.5	0.9974	0.997	5	85	0.9975
0.5555	0.9948		4	76	0.9949
0.6		0.992	4	71	0.9920
0.625	0.9898		4	68	0.9899
0.7		0.982	3	61	0.9818
0.7143	0.9798		3	60	0.9799
0.8		0.966	3	53	0.9664
0.8333	0.9600		3	51	0.9601
0.9		0.944	3	47	0.9460
1.0	0.9214	0.921	3	43	0.9216

The same results are obtained (to within 3 parts in 10^5) and the same number of terms are required if M is held constant at 20. Exact agreement with Smits is achieved if the condition that the residual be smaller than 10^{-6} is imposed but this more than doubles the number of terms in the series (4); the calculation is degraded if the seventh order terms are not used or if a residual larger than 10^{-5} is permitted.

For a finite specimen, the overall correction is estimated by multiplying together correction factors for the thickness (derived on the basis of an infinitesimally thin sheet of finite diameter). In view of the second-order error inherent in this procedure, refinement of the calculation for $G_7(w/\bar{S})$ beyond that given in eq (5) with a residual of 10^{-5} does not seem justified. (W. E. Phillips)

Temperature Coefficient of Resistivity — The applicability of previously calculated temperature coefficients [5] to correcting silicon resistivity data to reference temperatures other than 23°C was investigated at the request of the Resistivity Section of ASTM Committee F-1. From the data taken previously [5] on *n*-type and boron-doped silicon wafers, values of resistivity were calculated for each wafer at 1°C intervals for wafer temperatures from 15 to 30°C inclusive. These values were then corrected to 20, 23, and 25°C with the use of 1) the temperature coefficient experimentally determined for the wafers and 2) the temperature coefficient computed from the polynomial fit (NBS Tech. Note 560, pp. 6-8) to the temperature coefficient-resistivity curve. The corrected values were then compared with the calculated values derived from the data.

In all cases the corrected values of resistivity computed from the experimentally determined temperature coefficient for that wafer were within 0.1 percent of the calculated value if the difference between wafer temperature and reference temperature did not exceed 5°C. Similar results were found when the temperature coefficient computed from the polynomial fit was used. In the few cases where greater differences were observed between resistivities derived from the experimentally determined and computed coefficients, the errors introduced for correction to reference temperatures of 20 and 25°C were not significantly different from those for correction to a reference temperature of 23°C. In all of these cases the experimentally derived temperature coefficient did not fall on the smooth curve joining most of the data points.

From these results it was concluded that the temperature coefficient data derived for a reference temperature of 23°C could be used to correct resistivity measurements to 20 and 25°C without significantly reducing the precision of the measurement provided that the wafer temperature (during measurement) did not differ from the reference temperature by more than 5°C. (W. M. Bullis)

Standardization Activities — Data has been received and analyzed from six of the eight participants in the round robin sponsored by Committee F-1 to measure the resistivity of ultra-high resistivity silicon by the four-probe method. As expected, the greatest interlaboratory variation occured in general for the specimens which had the highest reported resistivity values. One laboratory had particular difficulty with *p*-type specimens, measuring well below the multi-laboratory average on all three *p*-type specimens. Difficulty with measuring the conductivity type of the specimens was encountered only on the specimen which had the highest average resistivity of all specimens considered. For this specimen, two laboratories measured both *n*- and *p*-type character.

Additional work done on this particular specimen indicates an extreme dependence of measured resistivity upon the method of surface cleaning and the time lapse between cleaning and measurement. Average

resistivities between 9100 and 18400 Ω·cm were obtained after various cleaning procedures. Details of the cause of this variability have not yet been established.

Data have been received and analyzed from six of the twelve participating laboratories in the round robin to measure the resistivity of epitaxial layers on opposite conductivity type substrates by the four-probe method. (F. H. Brewer)

Spreading Resistance Methods — The study of spreading resistance contacts has concentrated on use of the scanning electron microscope to examine probe damage in silicon. Although some high quality electron microscope pictures have been made on silicon surfaces after the surface received a gold deposition or was alloyed with gold, the results have not been fully reproducible. Because of lack of understanding of the relation between the conditions of probe lowering and the quality of the resulting spreading resistance contact, a search is being made for a suitable piezoelectric or other form of transducer that can be used to measure the impact momentum of the spreading resistance probe so that this quantity can be related to specimen surface damage and electrical stability of the contact. (J. R. Ehrstein)

Capacitance-Voltage Method — Diodes with more abrupt junctions than were attainable with previous procedures have been obtained by using a 3 h single-step boron diffusion at 1050°C. With this diffusion procedure, junction depth was increased from a planned value of 1 μm to about 2 μm, and breakdown voltages up to 40 V and 60 V, respectively, were obtained for 0.76-mm and 0.5-mm diameter diodes fabricated in nominal 1-Ω·cm, *n*-type silicon.

Capacitance measurements on these wafers are limited to diodes with high breakdown voltages. A comparison of the resistivities of three of the diffused *n*-type wafers as measured by the four-probe and capacitance-voltage (C-V) methods showed the C-V resistivity values to be consistently higher. The best agreement between four-probe and C-V resistivity measurements was obtained on the wafer that had the smallest radial resistivity variation. (G. N. Stenbakken and T. F. Leedy)

Plans: The evaluation of the effects of changes in the experimental procedure for the current and probe force dependence of resistivity as measured by the four-probe method will be completed and appropriate changes made. Data collection on mechanically polished wafers will be resumed. When the wafers from the ultra-high resistivity round robin are returned, work will begin on a comprehensive study of the effect of specimen surface preparation on the resistivity measurement of these wafers. Data from this and the epitaxial resistivity round robin will be computed and tabulated as received. Because of difficulties encountered in the resistivity inhomogeneity study (see Section 3.3) when wafers are

miscentered by only 100 μm or so during a four-probe resistivity profile, a mechanical wafer centering apparatus will be built.

A detailed study will be made on the necessary treatment to get repeatable, high-resolution SEM photomicrographs of probe damage in silicon. It will include a range of silicon resistivities of both conductivity types with both evaporated coatings and alloyed surfaces. Work will continue on finding a satisfactory transducer for measuring the impact momentum of the spreading resistance probe under various experimental situations. Results of this work will be related to the electrical stability of the contacts.

Four-probe resistivity profiles will be repeated on previously diffused 1-Ω·cm wafers to investigate whether the long diffusion times have in any way altered the radial resistivity profile on the original material. Diodes will be fabricated on additional 1-Ω·cm, *n*-type wafers with more uniform resistivity profiles than wafers previously used. Diodes will also be fabricated in 15-Ω·cm, float zoned, *n*-type wafers. These two groups of wafers will be used to investigate the diagreement between C-V and four-probe measurements of resistivity already observed for dependence on resistivity level and effect of resistivity profile.

3.2. CARRIER LIFETIME

Objective: To determine the fundamental limitations on the precision and applicability of the photoconductive decay method for measuring minority carrier lifetime and to develop alternative methods for measuring minority carrier lifetime in germanium and silicon which are more precise, more convenient, or more meaningful in the specification of material for device purposes.

Progress: Increased emphasis was placed on the study of the photoconductive decay method for measuring bulk carrier lifetime. The dependence of the measured value of lifetime on signal level, applied electric field, chopped-light turn-off time, and series resistance was established. An experiment to determine the relative single laboratory precision of the time-mark method and the null method for measuring photoconductive decay time was begun. The measuring circuit for the metal-oxide-semiconductor capacitance method for measuring carrier lifetime in epitaxial layers was calibrated, and initial measurements were carried out.

Previously observed variability in the measurement of the surface photovoltage was greatly reduced by shielding the specimen and thermopile from ambient room light. This new, non-contacting technique was successfully applied to the measurement of carrier diffusion length in silicon epitaxial layers.

Bulk Crystals — To expedite the revision of the PCD method, increased emphasis was placed on this measurement. A group of experiments was designed to study the dependence of the measured value of lifetime on PCD signal level, applied electric field, chopped-light turn-off time, and series resistance. The objective of these experiments was to accumulate data to determine appropriate test conditions for the revised PCD procedure, including methods of selection of the specimen current and signal level.

The decay time was studied as a function of the magnitude of the series resistance to determine a lower limit of the series resistance. For a group of four samples, decay time was measured for different values of the ratio of the series resistance to the specimen resistance (R_s/R) in the range 0.1 to 20. It was found that (1) the signal level decreased as R_s/R decreased, (2) the decay times measured at low R_s/R differed from those measured at high R_s/R, and (3) the magnitude of the standard deviation of the measurement varied randomly over the range of R_s/R despite the lower signal-to-noise ratio at low R_s/R. To ensure that the measured decay time is independent of the series resistance, a series resistance at least ten times the specimen resistance must be employed.

The dependence of the measured decay time on the turn-off time of the chopped light was studied to determine an upper limit for the turn-off time in terms of the ratio of turn-off time to PCD lifetime (t_{off}/τ_{PCD}). Five samples were measured for different values of t_{off}/τ_{PCD} in the range one to four. It was found that for $t_{off}/\tau_{PCD} < 2$, the measured decay time was approximately constant and equal to the PCD lifetime. To avoid influencing of the result by the time-off time, measurements must be made in this range. A transition occurred for t_{off}/τ_{PCD} between 2 and 3; for $t_{off}/\tau_{PCD} > 3$, the measured decay time increased with increasing turn-off time. For the conditions of measurement the transition point was calculated to be between 3.9 and 4. The discrepancy between the calculated and observed values is attributed to lack of sharpness in the turn-off characteristic of the light.

To study the effect of sweep-out, photoconductivity scans of eight specimens were made on the apparatus developed for studies of resistivity inhomogeneity (see Section 3.3). Since the photoconductivity is proportional to the lifetime, the fall of the photoconductivity near the end contacts is a measure of sweep-out. The electric field was normally selected to produce a drift length of about 1 mm. It was found that sweep-out always occurred within five drift lengths of the end contacts. Thus, masking the specimen so that the region within five drift lengths of the contacts is not illuminated is expected to avoid sweep-out.

The lifetime is a function of the injected carrier density, which can be related to the signal level. For a group of six samples, lifetime was measured at various signal levels. For these lifetime measurements

the relationship of the standard deviation to the signal level was studied. These data showed a clearcut difficulty in making precise lifetime measurements at lower signal levels, but a method for specification of the appropriate signal level has not yet been formulated.

Since sweep-out, ohmic heating of the specimen, current level, and signal level are interrelated, an experiment to study the effect of sample heating was initiated. The dependence of specimen temperature on the specimen current is being investigated for a group of fourteen samples. These samples cover the resistivity range 1 to 1500 Ω·cm.

To determine the relative precision of two methods for measuring the specimen voltage decay time two operators are measuring a single sample by both methods for an extended period. The first method consists of matching the PCD curve to an exponential curve inscribed on the oscilloscope graticule. The time constant of the matched curve is measured with a time-mark generator. In the second method, a differential oscilloscope input is used to match the PCD curve with an electronically-generated exponential curve. When the time constants of the two curves are equal, a null in the form of a straight line is formed. This experiment is still in progress. (A. J. Baroody and R. L. Mattis)

Epitaxial Layers — The measuring circuit for the MOS capacitance method was constructed, calibration was carried out, and initial lifetime measurements were begun. A computer program was written so that the transient capacitance data could be analyzed by the methods of Zerbst [1], Heiman [2], and Salama and Holmes [3]. Whereas the lifetime values calculated by the methods of Zerbst [1] and Salama and Holmes [3] were in agreement, the values calculated by the method of Heiman [2] differed from the others. This prompted a reexamination of the theory. It was found that the methods of Zerbst [1] and Heiman [2] are not entirely mutually consistent as suggested earlier (NBS Tech. Note 560, p. 12). Although the method of Zerbst [1] reduces to the method of Heiman [2] for the case in which surface charge generation is negligible, the two methods give different lifetime values when this condition is not met.

The first measurement was made on a 1-Ω·cm, *n*-type silicon wafer with an array of 1.25-mm diameter aluminum dots evaporated onto a 0.12-μm thick oxide layer. The capacitance *vs.* time data were fitted to polynomials of several orders, and the best polynomial fit was used to derive the lifetime value. It was found that the lifetime value depends on the bias voltages from which and to which the device is switched to produce the capacitance transient. This dependence is strongest in very shallow inversion. (R. L. Mattis)

The SPV equipment was modified to shield the specimen and the thermopile from ambient room light. Preliminary measurements indicate that the previously reported variability in the SPV measurements has been greatly reduced.

Analysis of the SPV method [4, 5] was extended to the case of an epitaxial layer on a thick substrate. The general boundary conditions [6, 7] at the epi-substrate interface simplify to a Boltzmann equation for n-on-n^+ or p-on-p^+ layers; the other boundary conditions are unchanged. The calculated expression for the SPV plot yields an approximately linear dependence of intensity on reciprocal absorption coefficient. For epitaxial layers thicker than several diffusion lengths, the results are the same as for thick specimens and the intercept gives a measure of the diffusion length in the epitaxial layer. For very thin epitaxial layers, less than half the diffusion length in the substrate, the intercept is equal to the diffusion length in the substrate. For layer thickness intermediate between these limits, the intercept is influenced by the layer thickness as well as the diffusion lengths both in the epitaxial layer and in the substrate. In principle, in this intermediate region the diffusion length in the epitaxial layer could be obtained from SPV measurements on both sides of the wafer. However, at present, the precision of the method is not adequate for such a determination. (W. E. Phillips)

Plans: Revision of the PCD procedure will continue. The data from the sweep-out, signal level, and current dependence studies will be evaluated to determine specifications for specimen current and signal level. The precision comparison between the time mark and the null methods of determining the specimen voltage decay time will continue. To compare these two techniques over a range of lifetime, a group of samples will be measured with both techniques.

Several specimens, including bulk and epitaxial specimens, will be measured by the MOS capacitance method. Agreement of repeated measurements will be evaluated for one or two specimens. Lifetime values derived from different polynomial fits to the same capacitance *vs.* time data will be compared. Lifetime values from two devices from different locations on the same wafer will be compared.

Additional SPV measurements will be made on other epitaxial layers to extend the experimental verification of the analysis. Also, SPV measurements will be made on several single-crystal specimens which have been previously measured by the PCD method in order to compare results obtained by the two methods.

3.3. INHOMOGENEITIES

Objective: To develop improved methods for measuring inhomogeneities responsible for reducing performance and reliability of germanium and silicon devices, and in particular, to evaluate a photovoltaic method as a means for measuring radial resistivity gradients in germanium and silicon circular wafers without contacting the flat surfaces of the wafers.

Progress: The analysis of the correlation between photovoltaic, four-probe, and two-probe profiles by the statistical techniques discussed previously (NBS Tech. Note 571, p. 13) was continued. Since correlation coefficients calculated by these techniques range from good (0.9) to quite poor (0 or negative), emphasis in the photovoltaic study is being placed on determining why the correlation of the resistivity profiles made by the different methods of measurement is very good for some wafers and very poor for others. In addition, greater care is now being taken to assure that both the photovoltaic and four-probe measurements are being made on the same wafer diameter and that the bar on which the two-probe measurement is made is cut accurately from that diameter.

An investigation into various factors which may affect the precision and accuracy of the resistivity profiles determined by each of the three measurement methods has been initiated. Two factors which strongly influence the four-probe method are the size of the resistivity gradient and the location (or the mis-location) of the probes on the specimen. Detailed study of the effect of uncertainty of probe location was begun. It was found that the calculated profile shape can be profoundly affected if the assumed probe positions are shifted by 100 μm or so.

Factors which may affect the photovoltaic resistivity profile are the resistivity gradient magnitude, the electrical quality (degree of non-ohmicity) of the measurement contacts, and non-radial resistivity gradients in the specimen. (D. L. Blackburn)

Preliminary work was begun on a plasma resonance technique that might be suitable for measuring resistivity inhomogeneity in low-resistivity wafers. The initial approach is either to modulate the specimen temperature or to place the specimen in a modulated magnetic field and use a phase sensitive lock-in detector to detect the plasma resonance minima. (D. L. Blackburn and W. R. Thurber)

Plans: The study of the effect of uncertainty of probe location on the four-probe method will be completed. Investigation of the effects of large resistivity gradients, non-radial resistivity gradients, and measurement contact quality on the photovoltaic method will continue.

Further work on the plasma resonance technique will be deferred until the present stage of the photovoltaic study is concluded and a report has been prepared.

3.4. GOLD-DOPED SILICON

Objective: To characterize *n*- and *p*-type silicon doped with gold and to develop a model for the energy level structure of gold-doped silicon which is suitable for use in predicting its characteristics.

Progress: Total gold concentrations, as determined by neutron activation analysis, in 10- and 20-Ω·cm, boron-doped, silicon wafers diffused at 850 and 1250°C are plotted in figure 1 as a function of diffusion time. These experiments were done to study the effects of crystal quality (dislocation density) and atmosphere on the gold diffusion process. The effect of a variety of atmospheres has been reported in the literature with conflicting claims as to the most suitable one. The results of the present study suggest that gold diffuses slightly faster in an oxygen atmosphere than it does in an argon atmosphere. It was also found that gold diffused faster in the high-dislocation wafers (20 Ω·cm) than it did in the low-dislocation wafers (10 Ω·cm). This result is in agreement with that of other workers.

It is known that gold accumulates at surfaces of wafers [1]. To avoid contributions to the neutron activation analysis determinations from such gold, both wafer surfaces are routinely lapped prior to activation analysis. Because some previously measured specimens were determined to have gold concentrations which could not be correlated with resistivity measurements (NBS Tech. Note 571, p. 15), contamination from gold accumulated at the rim of the wafer was suspected. Therefore in the present group, the rim was cut away from each of the specimens prior to activation analysis.

To test the hypothesis that gold accumulated at the rim might have influenced previous activation analysis results, the gold concentration was measured in both the center and rim portions of two specimens, one diffused at 1250°C for 4 h and the other at 850°C for 0.5 h. The concentrations measured in both the center and rim portions of the 1250°C specimen were about equal to the solid solubility of gold. In the case of the 850°C specimen, the rim portion had an average concentration 4 times the solid solubility while the center portion, because of the short diffusion time, had a concentration about 1/50th of the solid solubility. Because the rim portion also contained a significant volume in which the gold concentration was characteristic of the center portion it is clear that very large amounts of gold can accumulate at the rim. These results suggest that for specimens diffused at temperatures below 1250°C gold concentrations considerably in excess of the solid solubility at the diffusion temperature can be measured if the rims are not removed even though the gold concentration in the interior of the wafer may be equal to or less than the solid solubility. They also support the conclusion that the difficulties encountered previously in correlating measured gold concentration with electrical properties were probably due to the fact that the wafer rims had not been cut away prior to activation analysis.

To determine the lateral uniformity of the diffused gold, several specimens were examined by x-ray fluorescence with the scanning electron microscope. Examination of a diffused specimen from which the surface

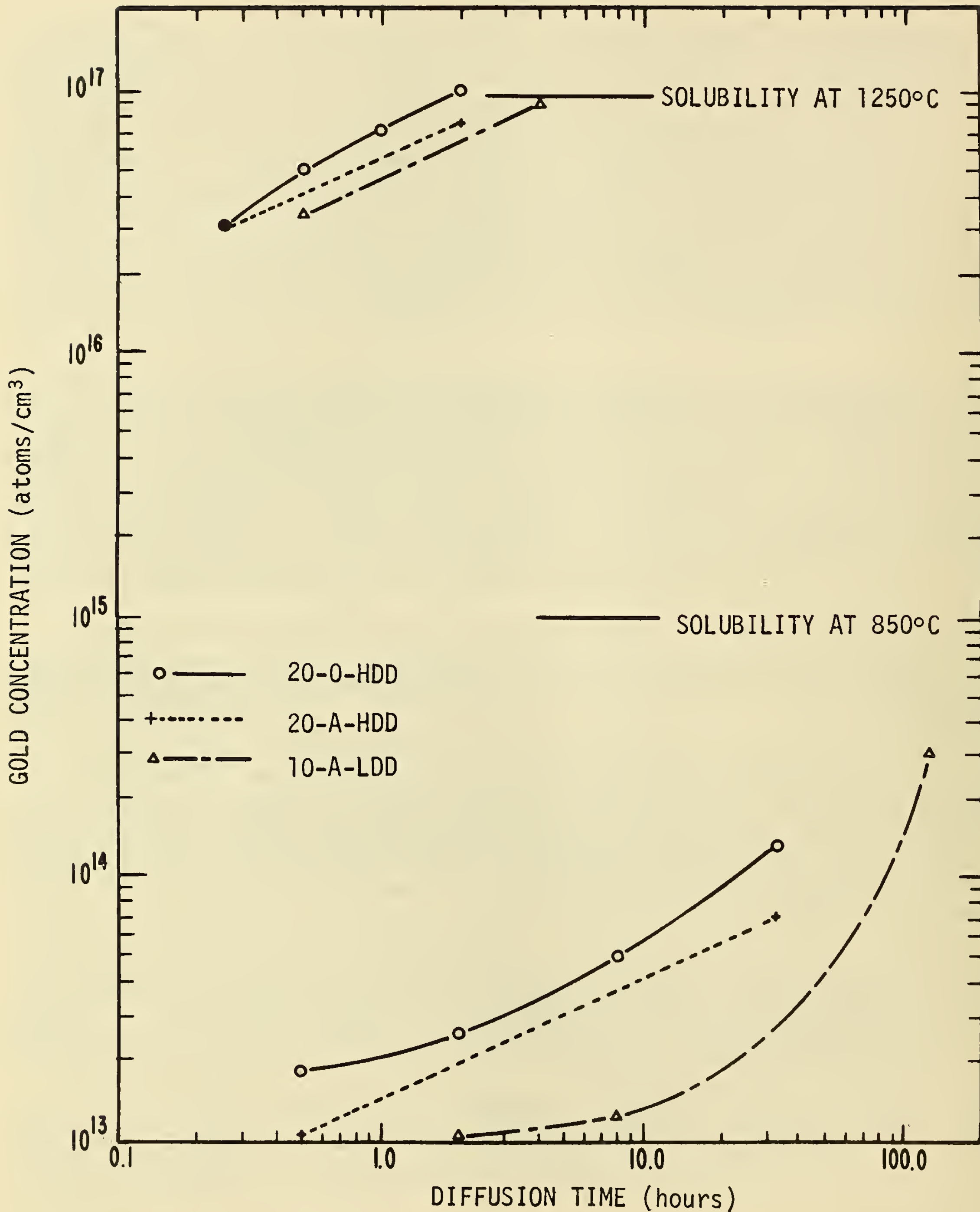

Figure 1. Gold concentration as determined by neutron activation analysis as a function of diffusion time for 10- and 20-Ω·cm, boron-doped, gold-diffused, silicon wafers. (The upper curves are for wafers diffused at 1250°C, the lower for wafers diffused at 850°C. The diffusion atmosphere was either oxygen (O) or argon (A). The 10-Ω·cm wafers had low dislocation density (500 cm^{-2}) and are indicated by LDD; the 20-Ω·cm wafers had high dislocation density (17,000 cm^{-2}) and are indicated by HDD. As diffused, the wafers were 1.1 mm thick; before activation analysis, 0.12 mm was lapped from each side and the rim was removed.)

gold had been removed by aqua regia showed clusters of gold, 2 to 5 μm in diameter near the surface. A piece of the same material with 0.06 mm lapped from the surface did not show any clusters.

Resistivity and Hall effect measurements were made at room temperature on Hall bars cut from the 10- and 20-Ω·cm, boron-doped wafers diffused with gold at 1250°C. For the set of four 20-Ω·cm specimens diffused in an oxygen atmosphere the gold concentrations ranged from 3.0 to 9.9 × 10^{16} atoms/cm^3 and the resistivity decreased with increasing gold concentration. Likewise for two 20-Ω·cm specimens diffused in argon the one with the higher gold concentration had the lower resistivity. Also of two 10-Ω·cm specimens diffused in argon, the one with the higher gold concentration had the lower resistivity. This retrograde behavior of the resistivity is not in agreement with theoretical predictions (NBS Tech. Note 520, p. 23) but is in agreement with previous measurements made elsewhere (W. M. Bullis, unpublished).

Spreading resistance measurements of a preliminary nature were made on an angle-lapped specimen to study the distribution of gold from the surface into the bulk of the wafer. Since gold was evaporated on both sides of the wafer before diffusion, a symmetrical profile was expected, but not observed. More work on this technique is needed before meaningful profiles can be obtained. (W. R. Thurber, T. F. Leedy, and W. M. Bullis)

Plans: More 10- and 20-Ω·cm, boron-doped silicon wafers will be diffused with gold to complete the range of gold concentrations for these resistivities. Also 90-Ω·cm, *p*-type wafers will be diffused at temperatures from 850 to 1250°C. Additional *n*- and *p*-type material will be selected and slices prepared for diffusion. Following gold diffusion, a part of each wafer will be sent for activation analysis and a Hall bar for electrical measurements will be cut from the remainder. Work will continue on the study of lateral and depth uniformity of the gold diffusions. Hall effect measurements as a function of temperature will be made on two or three of the 20-Ω·cm, gold-diffused, boron-doped specimens to determine if the ionization energy of the gold donor level at 0.35 eV above the valence band varies with gold concentration. If the ionization energy decreases as the gold concentration increases, then this may be a possible explanation for the retrograde behavior of the resistivity.

3.5. SPECIFICATION OF GERMANIUM

Objective: To measure the properties of germanium crystals and to correlate these properties with the performance of germanium gamma-ray detectors in order to develop methods for the early identification of crystals suitable for fabrication into lithium-compensated gamma-ray detectors.

Progress: Analysis of the data obtained in the evaluation of the lithium mobility and lithium precipitation methods for determining oxygen concentration in germanium has been completed, and the sensitivity and expected precision for each method determined. Several additional lithium-drifted germanium diodes have been examined by the improved infrared response technique. Response spectra have been obtained for a copper-doped specimen and another specimen without copper cut from the same crystal. The results show that the improved technique is capable of detecting impurities such as copper and identifying them by means of their observed energy levels.

Characterization of Germanium — Analysis and interpretation of data obtained in the study of lithium mobility and lithium precipitation as a means of measuring oxygen concentration in germanium have been completed. In figure 2 oxygen concentration as determined from both lithium precipitation and infrared absorption measurements is plotted against oxygen concentration determined from measurements of lithium-ion drift mobility. The error bars shown for some of the points represent an estimate of the precision of the measurements: ±30 percent for lithium mobility, ±45 percent for lithium precipitation, and ±60 percent for infrared absorption. The precision statements for the lithium mobility and lithium precipitation methods are based on repetitive, single-laboratory measurements on specimens with oxygen concentration between 0.2 and 20 ppb atomic (10^{13} and 10^{15} atoms/cm^3) and represent three relative standard deviations. The precision statement for the infrared absorption method is based on a multi-laboratory round-robin test [1] and also represents three relative standard deviations.

The straight line was obtained from a least squares fit to the solid data points where the three solid points for which error bars are shown have been ignored in the fitting procedure. These three points were rejected as outliers with a 1 percent risk that they really belonged to the group [2]. The slope of the line shows that determination of oxygen concentration by measurements of lithium precipitation and lithium mobility differ by less than 10 percent. Since the infrared absorption technique relates to oxygen in germanium through the unique 11.7-μm absorption band, the measurements of oxygen concentration by infrared absorption were used to verify that the lithium mobility and precipitation methods were also measuring oxygen concentration. That this is so can be seen by the coincident relationship between the solid and open data points.

(A. H. Sher, W. K. Croll, and W. R. Thurber)

Ge(Li) Detector Measurements — Infrared response (IRR) spectra [3] of three Ge(Li) detectors at about 100 K have been studied in detail. Spectra of these diodes obtained with a 3-mm thick germanium filter are shown in figure 3. Ge(Li) 13Cu was fabricated from a portion of crystal NBS-13 which had been diffused with copper at 750°C for 12 days, Ge(Li) 13 was fabricated from a portion of crystal NBS-13 which had been

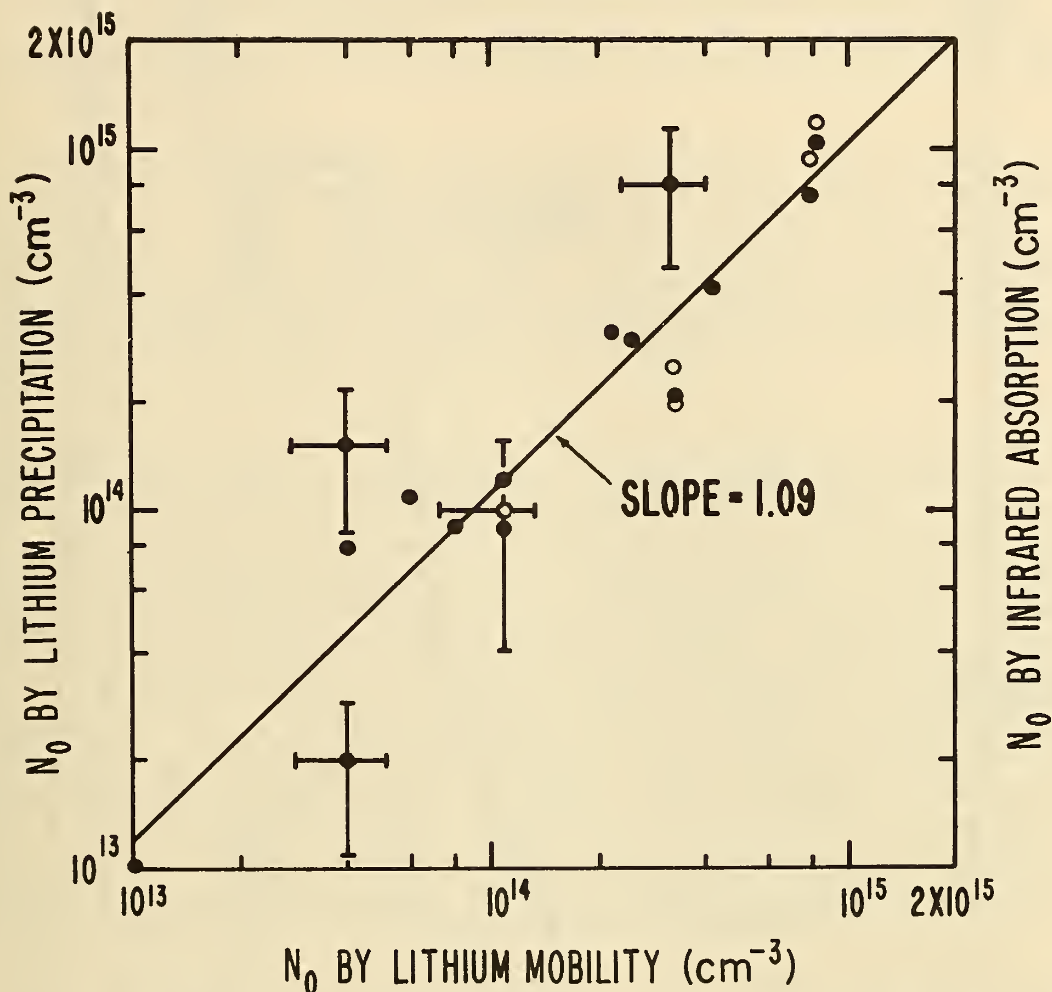

Figure 2. Oxygen concentration, N_0, obtained from lithium precipitation (●) and infrared absorption measurements (○) plotted against N_0 obtained from lithium mobility measurements. (The error bars represent three standard deviations (see text).)

subjected only to the normal detector fabrication procedure, and Ge(Li) 83-3 was fabricated from crystal NBS-83. The IRR spectrum taken with a 1-mm thick germanium window on another detector fabricated from crystal NBS-83 was indicative of many discrete levels in the forbidden energy gap (NBS Tech. Note 571, pp. 16-18).

According to previous studies [3], the interpretation of the prominent features displayed by the spectra would indicate that both Ge(Li) 83-3 and Ge(Li) 13 contain "lithium-defect" electron traps as indicated by the shelf-like response at 0.50 eV. Another Ge(Li) detector fabricated

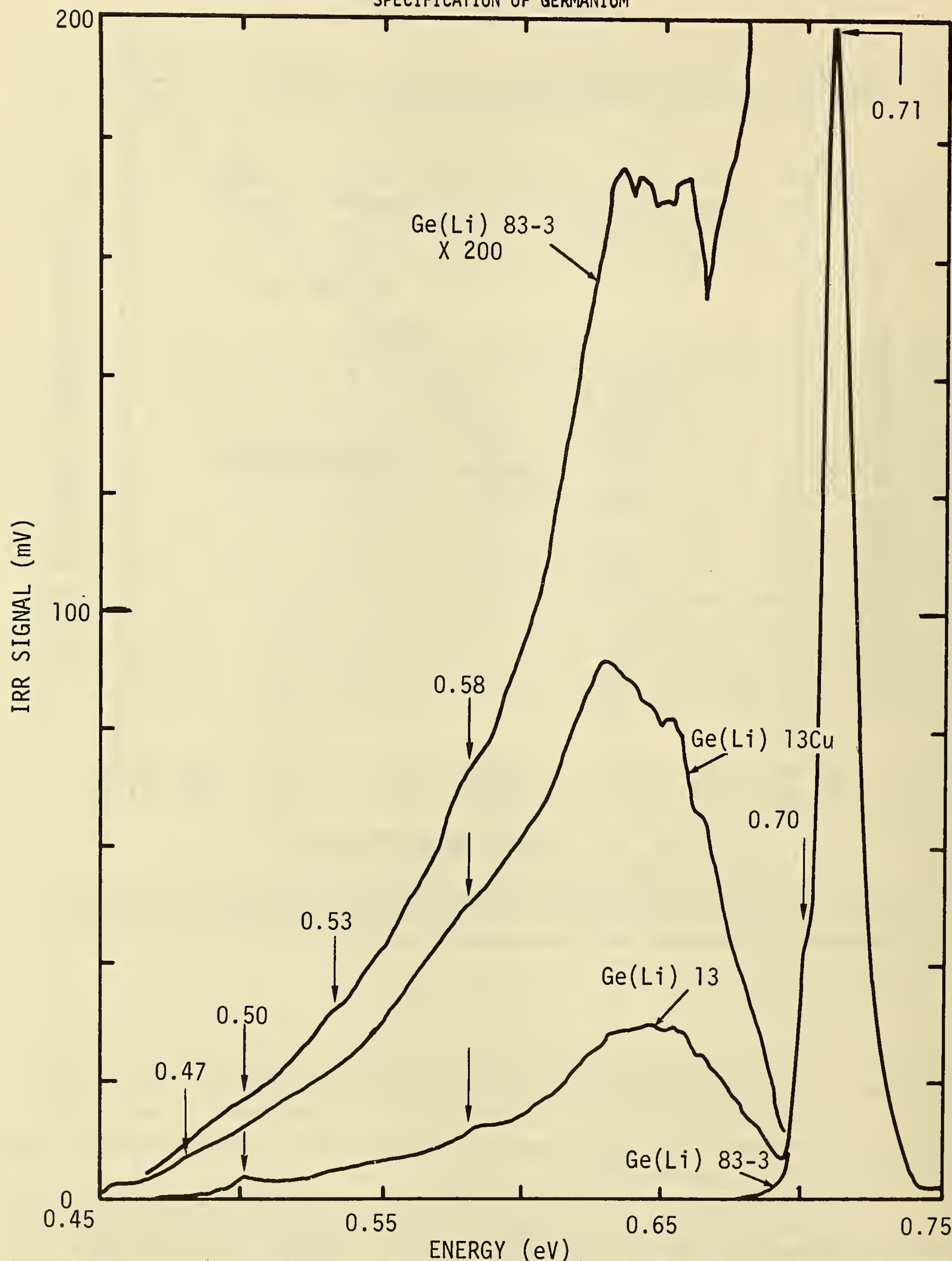

Figure 3. Infrared response (IRR) spectra obtained using a 3-mm thick germanium filter. (Specimen Ge(Li) 13Cu contains approximately 10^{14} copper atoms/cm^3. All spectra have been normalized to the band-edge response peak (at 0.71 eV); a portion of the IRR spectrum for Ge(Li) 83-3 is shown at a sensitivity level increased by a factor of 200 over the others. Specimen temperature was about 100 K. A 640 line/mm grating was employed.)

from crystal NBS-83 showed slight electron trapping in previous studies made with a collimated gamma-ray beam (NBS Tech. Note 495, pp. 18-19). Ge(Li) 13 is expected to show much more severe electron trapping due to the increased magnitude of its IRR response, but this has not as yet been confirmed experimentally.

The IRR spectrum of Ge(Li) 13Cu shown in figure 3 does not exhibit any features which were previously attributed to the presence of copper in a crystal [3]. On the basis of this IRR spectrum one would predict that the detector should exhibit severe carrier trapping characteristics, but the type of trap cannot be specified. Measurements of resistivity of the copper-diffused portion of crystal NBS-13 showed that approximately 10^{14} cm^{-3} electrically active impurities had been introduced into the crystal.

The results become less ambiguous when a 1-mm thick germanium filter is used. Figure 4 shows IRR spectra for incident infrared radiation of energy between 0.30 and 0.70 eV obtained for the three cyrstals under study. These curves are plotted on a semi-log scale to indicate the relative signal magnitudes obtained during a spectrum scan, and to aid comparison of data between specimens. The curves have been plotted so that the levels of the minimum detectable signal coincide. The semi-log display of the spectra, it should be noted, causes some of the features to be seen in less detail than on the linear scale as normally obtained from the experiment. The overall signal level of Ge(Li) 13Cu is an order of magnitude greater than that of Ge(Li) 13. The spectrum of Ge(Li) 13Cu exhibits two features not seen in the other curves, a peak at 0.38 and a knee at 0.49 eV. These correspond to the copper levels at E_v + 0.33 eV and E_c - 0.22 eV, respectively. Analysis of the gamma-ray characteristics of Ge(Li) 13Cu determined using a collimated gamma-ray indicated severe hole trapping as is predicted for copper-doped germanium [3].

IRR studies previously performed using a 3-mm thick germanium filter [3] gave no indication of the presence of a number of the discrete energy levels observed with a 1-mm thick filter in the present work. This can probably be accounted for by differences in the spectral transmission of the 1- and 3-mm thick germanium filters; there is a much decreased absorption of radiation of energy between 0.65 and 0.70 eV when the 1-mm thick filter is used. Scattering of this high energy radiation in the monochromator may make it possible for optical pumping of the levels to occur when using a 1-mm thick filter [5], and so many of the discrete levels unobserved using the 3-mm thick filter can be excited. The peaks at 0.36 eV and others observed at 0.24 and 0.18 eV (not shown) appear to result from band-edge radiation which occurs because of higher order diffraction. Although radiation of this energy is filtered out, it is not completely eliminated. Since the detectors are much more sensitive to it than to lower energy radiation, a signal can be seen.

(A. H. Sher, W. J. Keery, and H. E. Dyson)

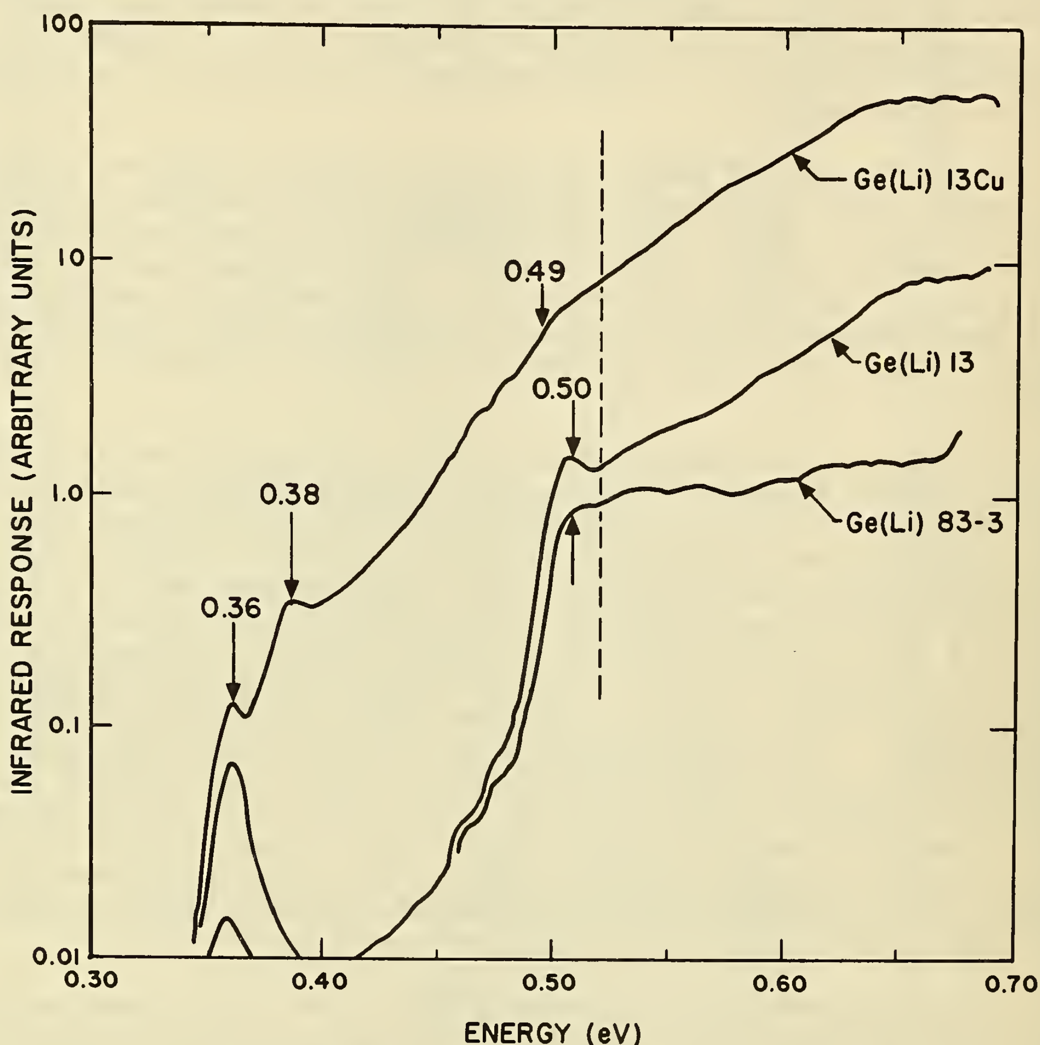

Figure 4. IRR spectra in the incident photon energy range of 0.30 to 0.70 eV obtained using a 1-mm thick germanium filter. (The spectra are plotted so that the levels of minimum detectable signal coincide. To the right of the vertical dashed line a 640 line/mm grating was used; to the left, a 240 line/mm grating. In all cases specimen temperature was about 100 K.)

Plans: Study and correlation of measurements of lithium driftability, infrared response, and distribution of etch pits, three of the most promising methods for characterizing germanium for Ge(Li) detectors, will continue with the aim of developing one or more of these methods into a meaningful test for the rapid and proper specification of detector-grade germanium. Additional specially doped crystals will be examined along

with heat-treated and radiation-damaged crystals in order to aid the interpretation of the results of the improved IRR measurements. Measurement and interpretation of Ge(Li) detector characteristics with standard experimental methods and theoretical models will be continued.

3.6. REFERENCES

3.1. Resistivity

1. Smits, F. M., Measurement of Sheet Resistivities with the Four-Point Probe, *Bell System Tech. J.* 37, 711-718 (1958).

2. Uhlir, A., The Potentials of Infinite Systems of Sources and Numeriial Solutions of Problems in Semiconductor Engineering, *Bell System Tech. J.* 34, 105-128 (1955).

3. Valdes, L., Resistivity Measurements on Germanium for Transistors, *Proc. IRE* 42, 420-427 (1954).

4. These values, obtained by linear interpolation from Smits' table, are those quoted in Method for Measuring Resistivity of Silicon Slices with a Collinear Four-Probe Array (ASTM Designation: F84-70), *Annual Book of ASTM Standards*, Part 8, Am. Soc. for Testing and Materials, Philadelphia, Pa., 1970, pp. 746-760.

5. Bullis, W. M., Brewer, F. H., Kolstad, C. D., and Swartzendruber, L. J., Temperature Coefficient of Resistivity of Silicon and Germanium near Room Temperature, *Solid-State Electronics* 13, 639-646 (1968).

3.2. Carrier Lifetime

1. Zerbst, M., Relaxationseffekte an Halbleiter-Isolator-Grenzflächen, *Z. Angew. Phys* 22, 30-33 (1966).

2. Heiman, F. P., On the Determination of Minority Carrier Lifetime from the Transient Response of an MOS Capacitor, *IEEE Trans. Electron Devices* ED-14, 781-784 (1967).

3. Salama, C. A. T., and Holmes, F., On the Determination of Surface Recombination Velocity from the Transient Response of MIS Structures, *Solid-State Electronics* 13, 1204-1205 (1970).

4. Goodman, A. M., A Method for the Measurement of Short Minority Carrier Diffusion Lengths in Semiconductors, *J. Appl. Phys.* 32, 2550-2552 (1961).

5. Bergmann, F., Fritzsche, C., and Riccius, H. D., Bestimmung der Diffusionslange in Halbleitern mit Hilfe des Oberflachemphoto-effektes, *Telefunken Ztg.* 37, 186-193 (1964).

6. Harrick, N. J., Characteristics of Junctions in Germanium, *J. Appl. Phys.* 29, 764-770 (1958).

7. Fletcher, N. H., General Semiconductor Junction Relations, *J. Electronics* 2, 609-610 (1957).

3.4. Gold-Doped Silicon

1. Boltaks, B. I., Kulidov, G. S., and Malkovich, R. Sh., The Effect of Gold on the Electrical Properties of Silicon, *Soviet Physics — Solid State* 2, 167-175 (1960).

2. Sprokel, G. J., and Fairfield, J. M., Diffusion of Gold into Silicon Crystals, *J. Electrochem. Soc.* 112, 200-203 (1965).

3. Martin, J., Haas, E., and Raithel, K., Radiochemische Untersuchungen zur Diffusion von Gold in Silizium, *Solid-State Electronics* 9, 83-85 (1966).

3.5. Specification of Germanium

1. Quoted in Method of Test for Interstitial Atomic Oxygen Content of Germanium by Infrared Absorption (ASTM Designation F 122-70T). *Annual Book of ASTM Standards,* Part 8, Am. Soc. for Testing and Materials, Philadelphia, Pa., 1970, pp. 885-886.

2. Natrella, M. G., *Experimental Statistics,* NBS Handbook 91, rev. ed., p. 17-3, 1966.

3. Armantrout, G. A., Infrared Evaluation Techniques for Ge(Li) Detectors, *IEEE Trans. Nucl. Sci.* NS-17, No. 2, 16-23 (1970).

4. McElroy, J. M., Photoconductivity — An Instructive Exercise in Semiconductor Theory, *IEEE Trans. Ed.* E-11, No. 1, 12-18 (1968).

5. Armantrout, G. A., private communication.

4. METHODS OF MEASUREMENT FOR SEMICONDUCTOR PROCESS CONTROL

4.1. METALLIZATION EVALUATION

Objective: To improve methods for measuring the properties of thin metal films with initial emphasis on the adhesion of aluminum metallization deposited on various substrates.

Progress: An exhaustive series of scratch tests was made on a 1.03-μm thick aluminum film deposited on a quartz substrate. This was one of a batch of substrates which was prepared by vacuum evaporation immediately after cleaning and degreasing. Previously, substrates had been prepared similarly except that they were heat treated in air at about 850°C just prior to vacuum evaporation. Three diamond styli with nominal tip radii of 18 μm, 45 μm, and 120 μm were used to scratch the films.

With the 45-μm stylus, the load was varied from 40 to 300 g. Threshold adhesion failures of the type described earlier (NBS Tech. Note 527, p. 23) were not observed here. Although the initial measurements were made when the film was but two days old, the film behaved as though it were a fully aged, highly adherent film. Under the stylus the film was progressively thinned with increasing stylus load, as evidenced by the translucency of the scratch. Although translucency was detectable under microscopic observation at a magnification of 200 X after scratching with an 80-g load, there was no optical evidence of the transparency indicative of complete film removal, even at loads as high as 300 g. Similar observations, considered to be characteristic of highly adherent aluminum films, have been reported by Collins [1].

Scratches with the 120-μm stylus were made with the loads ranging from 100 to 1100 g. As the loads increased, there was a corresponding increase in track width, but thinning of the film was insufficient to allow detectable translucency. Only a few clear threshold adhesion failures were observed at loadings of 1000 and 1100 g. Crescents (NBS Tech. Note 571, p. 22) were observed in abundance. Frequently thin, translucent spots or breaks were closely associated with these crescents, but the breaks were not of threshold failure type.

The crescents observed here were first observed in a 0.5-μm thick aluminum film in scratches also produced by a 120-μm stylus. It was suspected that these might be due to fracture of the quartz substrate. Experiments were carried out to estimate the lowest load required on a stylus so that it would leave an identifiable permanent deformation on a quartz substrate, without an interposing aluminum film. For a 120-μm stylus on fused quartz, it was found that crescent shaped fractures were produced along the scratch path with a 140-g load. With increasing stylus loads, many groups of crescent fractures were generated, frequently

including complete circular fractures. This tends to confirm the belief that a crescent observed in a scratch on an aluminum film is associated with a crescent fracture in the substrate directly beneath it. It would seem possible then, that crescent-shaped thin spots or breaks observed in aluminum films at higher loads may be brought about by the thinning down and deformation of the film over the crescent fracture in the substrate. Since the scratch test fails when the substrate suffers destruction, it follows that breaks or failures in the film connected with crescents are not threshold adhesion failures and are therefore set aside. It is interesting to note that Hamilton and Rawson [2] have very recently reported similar fracture results for a steel ball sliding on a glass plate.

Loads in the range 30 to 120 g were used for scratching with the 18-μm stylus. Progressive thinning with increasing load took place, and translucency was detectable at a stylus loading of approximately 40 g. It is to be emphasized that (1) any one scratch is not uniformly translucent, (2) the number of translucent streaks usually varies from track to track and often within a single track, (3) the light transmission of any one translucent streak may change discontinuously along its length, and (4) the scratch is not transparent.

However, within the scratches made with the 18-μm stylus many spots appeared to be significantly brighter than the surrounding translucent region, and to have a distinct white-light diffraction pattern associated with them. These spots strongly resembled previously observed threshold adhesion failures, although they were decidedly smaller. Since the diffraction pattern was present, it is believed that these tiny brighter spots are transparent holes in the film and represent failure points. That the occurrence or non-occurrence of these spots was quite distinct with rather small differential stylus loadings is taken as further evidence of this conclusion.

On the basis that the tiny bright spots within associated diffraction patterns are threshold adhesion failures, a number of measurements were made to determine sensitivity and reproducibility. The usual up-and-down method was applied. From the results, shown in table 2, it can be seen that the test can distinguish between failure and non-failure for a differential load of 2.0 g. Thus for this particular 1-μm thick film a sensitivity of approximately 4 percent is indicated. Although this sensitivity is considerably lower than values reported previously for 0.5-μm films, it by no means represents the ultimate value expected for 1-μm thick films.

Runs 1 through 3 were interdigitated. If the differences in load increment are ignored and the data are treated together, the grand mean failure load is 57.6 ± 1.8 g. If the data are assumed to be normally distributed it can be asserted with 95 percent confidence that the relative standard deviation for the entire population is less than 14 percent.

Table 2 — Results of Scratch Tests on a 1.0-μm Thick Aluminum Film with an 18-μm Diamond Stylus

Run No.	Load Increment (g)	Mean Failure Load (g)	Sample Standard Deviation (g)
1	5.0	59.2	10.0
2	2.0	57.9	4.4
3	2.0	55.7	2.0
4	2.0	59.0	4.8
Grand Mean (1-3 only)		57.6	1.8

Although aging effects had been observed in earlier measurements, measurements on specimen B6-S1 (1 μm thick) revealed no evidence of any increase in adhesion due to aging. It is possible that omission of the heat treatment may be responsible for the lack of aging effects and for the high adherence of this film. It is also possible that the lack of observed aging effects may be characteristic of films of this thickness; previously reported [3] aging effects were observed on much thinner films.

A parallel effort was undertaken to determine the feasibility of detecting threshold adhesion failure in the aluminum-silicon dioxide-silicon system. One approach is to use an infrared sensor such as PbS. Built into a suitable microscope system, the PbS detector probably holds the best promise for an automated apparatus. A second approach which was investigated in more detail involves the use of an infrared imaging tube combined with a microscope.

All commercial infrared imaging tubes use the same sensing element known as an S-1 photocathode. Although its sensitivity falls off very rapidly in the silicon transmission band (1.2 to 1.5 μm) it appears that sufficient signal is available in that range to permit viable instrumentation. An important advantage of the imaging tube approach is that the detector is very sensitive in the visible, thereby allowing an investigator to inspect the specimen from above and make necessary mechanical adjustments.

The capabilities of an infrared imaging tube were explored using a 0.5-μm thick aluminum film on quartz with known failure points and a glass filter which filtered out all the visible radiation. An available imaging tube was mounted on the microscope ordinarily used for scratch

test observations (objective magnification: 11 X). Under these experimental circumstances, only the larger failure points were observable. Very small failure points, several micrometers or less in diameter, were not resolvable.

A similar film specimen and a silicon wafer for use as an infrared filter were submitted to a vendor of an infrared imaging microscope to determine the capabilities of his instrument. He reported no difficulty in seeing even the smallest holes in the aluminum film.

(J. Oroshnik and W. K. Croll)

Plans: Future work on this task will be redirected toward other techniques more directly applicable to the determination of adhesion of bonding pads and the effect of bonding-pad adhesion characteristics on bond strength.

4.2. DIE ATTACHMENT EVALUATION

Objective: To evaluate methods for detecting poor die attachment in semiconductor devices with initial emphasis on the determination of the applicability of thermal measurements to this problem.

Progress: Measurements of thermal resistance and transient thermal response were made on 20 diode chips bonded to TO-5 headers. In all the devices a silicon-gold eutectic die bond was employed. Heat for the measurements was generated by pulses of power ranging from 100 μs to 5 s in duration. The duty cycle was such that the junction temperature cooled to an equilibrium value, the case temperature, during the period that heating power was not applied. A typical transient thermal response curve for these devices is shown in figure 5. The curve depicts the diode-junction-to-case temperature difference, ΔT_{JC}, normalized to its steady-state value as a function of the heating-power pulse width. The junction temperature was determined during the heating-power off period from the forward voltage, V_F, of the diode at 1 mA. The calibration of V_F with respect to temperature was obtained by externally heating the case and measuring the forward voltage at 1 mA. This current is not sufficient to alter the junction temperature significantly.

A mesa diode on a 0.95-mm square chip mounted on a TO-5 header typically exhibited 60°C/W thermal resistance. The theoretical thermal time constant for a device with junction-to-bonding-surface thickness of 0.25 mm (0.01 in.) is approximately 500 μs [1]. Since it is necessary for the chip to reach thermal equilibrium to maximize the amount of heat reaching the chip bonding surface, a heating pulse of 5 to 10 thermal time constants is expected to result in maximum sensitivity of the thermal response measurement to voids in the die attachment (NBS Tech. Note 555,

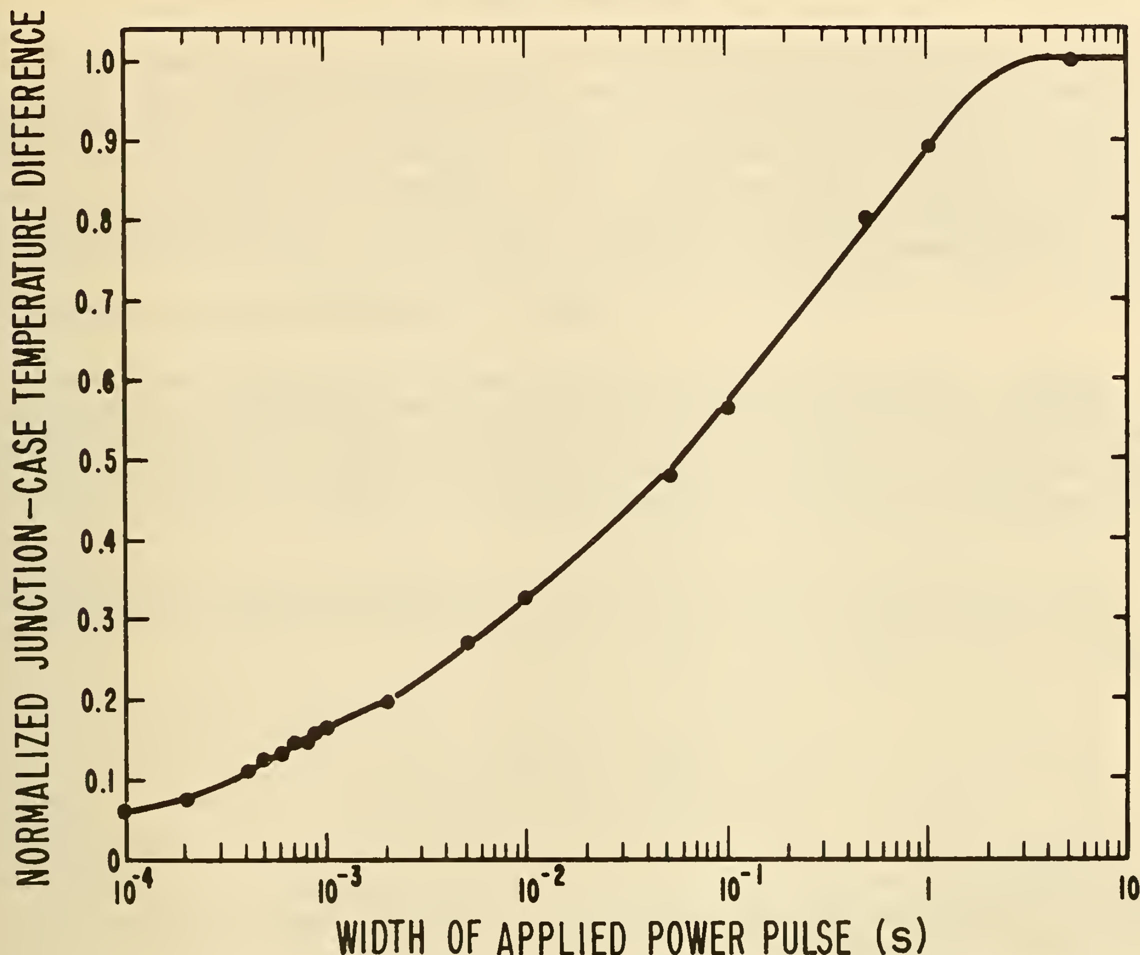

Figure 5. Transient thermal response curve for a typical mesa diode on a 0.95-mm square chip mounted on a TO-5 header. (Diode junction-to-case temperature difference normalized to its steady-state value is plotted as a function of the heating power pulse width. The case temperature was held at 25°C. For this diode the steady-state value corresponds to a thermal resistance of 60°C/W.)

pp. 25-27). Initial measurements of the transient thermal response indicate that a 5-ms, 800-mA heating power pulse produces an increase in the junction temperature of 10 to 12°C which is sufficient for reproducible measurements of ΔT_{JC}. Increased sensitivity is attainable by increasing the heating current. However, under such conditions the accuracy of the measurement is reduced because of an increased delay in the measurement of the forward voltage drop which is necessary since the higher heating current being switched increases the masking effect of electrical transients on the thermal transients.

Preliminary measurements of both thermal resistance and transient thermal response were made on five devices to check the reproducibility

of the die attachment evaluation equipment. The results of two runs of measurements taken 10 and 50 μs after the termination of the 5-ms heating power pulse indicate that the measurements of ΔT_{JC} for both transient and steady state operating conditions can be reproduced to within 1°C for any particular device. The variation in ΔT_{JC} between the five devices for a particular run was a maximum of 2°C. As expected, the longer the delay time before measuring V_F, the smaller is the ΔT_{JC} for a given heating current due to conduction cooling of the diode junction.

(F. F. Oettinger and R. L. Gladhill)

Plans: Long-term, single-operator measurements will be undertaken to check the reproducibility of the die attachment evaluation equipment. Measurements of thermal response will be undertaken to determine the sensitivity of the junction-to-case temperature change as a function of the magnitude of the diode heating current for a heating power pulse width of 5 ms and for direct current.

The fabrication of diodes with various diameter controlled voids will continue and measurements of thermal resistance and transient thermal response will be undertaken on these diodes.

4.3. WIRE BOND EVALUATION

Objective: To survey and evaluate methods for characterizing wire bond systems in semiconductor devices and where necessary to improve existing methods or develop new methods in order to detect more reliably those bonds which eventually will fail.

Progress: Study of the effect of pull rate on the pull test revealed that when the failure occurred at the heel of the first bond pulling at a rate of 77 gf/s (764 mN/s), equivalent to the "jerk" test used by some device manufacturers, gives results statistically equivalent to pulling at a rate of 1 gf/s (9.8 mN/s). The importance of specifying all details of the test including the wire bond failure mode has become apparent. Tests carried out to simulate the high temperature environment encountered by bonds during glass sealing operations for ceramic packages showed that the reduction in pull strength can be accounted for principally by the reduction in wire tensile strength caused by the high temperature anneal.

Improvements in the laser mount for interferometry measurements were made to increase the ease of optical alignment and use of the interferometer on bonding machines. The length of the laser was increased in order to limit all emission to the TEM_{00} mode.

New experiments directed toward development of measurement methods applicable to in-process bond quality determination were started. The initial effort consisted of electronically mixing the 60-kHz output from a capacitor microphone directed at the bonding tool with a local oscillator. Preliminary results showed that the bonding process can be heard through an audio speaker and recorded on magnetic tape. Harmonics of the 60-kHz tool motion can be individually treated in the same manner.

The wire indentation tester is nearing completion.

Pull Test Evaluation — It was previously reported (NBS Tech. Note 560, p. 31) that the rate of pull had no significant effect on the measured values of pull strength for pull rates of from 1.0 to 12.5 gf/s (9.8 to 122 mN/s) for single-level bonds, where the mode of failure is a break at the heel of the first bond. Two extensions of this work were considered: (1) faster rates of pull to simulate a "jerk test" which is used by some device manufacturers, and (2) the effect of pull rate on measured bond strength for the case where the failure mode is peeling or lift off of the bond.

Groups of 60 bonds each were pulled at rates of 1.0 and 77 gf/s (9.8 and 764 mN/s) resulting in times of approximately 9 and 0.12 s to pull a bond, respectively. The bonding schedule was such that failure occurred at the heel of the first bond in all cases. There was no statistically significant difference in the measured pull strengths for either pull rate.

For bonds that fail by peeling, it is assumed that the rate of pull would have a large effect on the measured pull strength since peel failure is known to be rate sensitive. However, it is very difficult to show this statistically, using the measured pull strengths. Up to the present, a procedure to make bonds reproducibly that will fail by peeling has not been found. Attempts thus far have resulted in bond strengths that have greater variations from bond to bond, at a given pull rate, than between groups pulled at different rates. Therefore, a pull-rate experiment as just described cannot now be performed for bonds that fail by peel. Nevertheless it seems clear that the nature of the failure mode may affect comparisons of pull strength and rates of pull.

It should be noted that all pull rate tests previously described were performed on single-level bonds. These results have not yet been verified for the case of two-level bond pairs such as are usually made on packaged devices. There may be some differences because the resolution of forces for this configuration tends to favor the lift-off failure mode for one of the bonds. (K. O. Leedy and C. A. Main)

Bond pull tests are often made on devices which are heat treated during the package sealing operation. For the case of glass-sealed,

ceramic packages, bonds are subjected to about 500°C for relatively long periods of time. In order to evaluate the effect of this process on the bond strength an experiment was designed to test both the bond and the wire before and after exposure to high temperatures.

Two hundred single-level bond pairs were made in sequence by one operator using identical machine settings. Every other bond pair was pulled to destruction and the average pull strength determined. The substrate with the remaining bonds was placed in a nitrogen atmosphere at 505°C for 20 min. These annealed bond pairs were then pulled to destruction. Before heating, the average pull strength was 9.3 ± 0.66 gf* (91 ± 6.5 mN); 87 percent of the bonds broke at the heel of the first bond, and none broke in the span of the wire. After heating, the average pull strength was only 4.5 ± 0.38 gf* (44 ± 3.9 mN), and 80 percent of the bonds broke in the span of the wire while only 16 percent broke at the heel of the first bond.

To see how much influence annealing the wire has on the bond pull strength, unbonded wire samples were given heat treatment identical to that of the bond pairs described above. The ends of the wire samples were mounted in epoxy cement and the wire was pulled to destruction using the hot-melt glue puller (NBS Tech. Note 488, pp. 22-23). The unheated wire had an average breaking strength of 12.0 ± 0.33 gf* (117 ± 3.2 mN). The annealed samples had a breaking strength of only 3.5 ± 0.35 gf* (34 ± 3.4 mN). (K. O. Leedy and C. A. Main)

A resolution-of-forces calculation (NBS Tech. Note 555, p. 33) of the tensile force, T, applied to the annealed wire bond pair during pulling was made using the measured loop height, 0.017 to 0.018 in. (0.43 to 0.46 mm), and bond length, about 0.04 in. (1.0 mm).† The calculated tensile force, T_{wt}, in the wire of a bond pair having a pull strength of 4.5 gf (44 mN) was 3.4 gf (33 mN), almost identical to the separately measured wire breaking strength. This suggests that if a wire bond loop breaks in the wire span, the breaking strength can be used to

---

* The range given is one sample standard deviation.

† For accuracy in the calculation for the case of annealed wire, it is essential that the loop height be measured after the wire is stretched by the pull test apparatus because wire annealed at high temperatures undergoes very large elongation that may add as much as 0.002 or 0.003 in. (0.05 to 0.07 mm) to the loop height. This may result in a different distribution of forces at the time of breakage. One way of forming the loop so that it can be measured after stretching is to push the wire segments carefully back together after the bond is pulled. Another is to tension the bond on the pulling apparatus to a force slightly less than that required to break adjacent bonds.

calculate the tensile strength of the wire on the basis of a simple resolution of forces. This is in contrast to the result found when the bond fails at the heel of the first bond (NBS Tech. Note 571, pp. 24-26).

Using the same resolution of forces equations, the loop height that will result in $T_{wt} = T$ was calculated for the various bond lengths that are normally used in this laboratory. Use of the appropriate loop heights in the future would permit the reported bond strength to be the same as the tension in the unannealed wire at the moment of rupture. As an example, for a bond length of 0.04 in. (1 mm) in a single level bonding situation the loop height for $T_{wt} = T$ is approximately 0.012 in. (0.3 mm). (G. G. Harman)

Some organizations seal at temperatures slightly below 500°C. Under these conditions it is observed that the majority of the bonds break at the heel rather than in the span. This was confirmed by performing a second experiment with 10 single-level bond pairs. After pulling every other bond pair to destruction the substrate with the remaining bonds was placed in a nitrogen atmosphere at 490°C for 20 min. The annealed bond pairs were then pulled to destruction. The average pull strengths and standard deviations before and after heating were similar to those found in the 505°C experiment. Again, before heating, no bonds failed in the span. However, after heating only 40 percent of the bonds broke in the span as compared with 80 percent for the 505°C experiment. This result is in accord with the known fact that metallurgical changes take place in the wire around 500°C. (K. O. Leedy and C. A. Main)

Characterization of Ultrasonic Wire Bonding Systems — The laser interferometer system [1] previously described (NBS Tech. Note 555, p. 30, and NBS Tech. Note 571, p. 31), has been greatly improved in its convenience of operation. The laser is now mounted on a stabilized, portable tripod platform having x-, y-, and z-axis micrometer positioners as shown in figure 6. The interferometer output is displayed on an oscilloscope not shown in the figure. The system can now be set up and optically aligned on any bonding machine or experimental setup in approximately 5 min. A complete calibration of bonding tool tip vibration amplitude as a function of power supply control setting takes only 5 to 10 min of additional time.

When using the above system the laser is not physically attached to the bonding machine. Therefore, small, low-frequency room vibrations, of the order of several microinches, will change the output waveshape at the end or turn-around points of the tool motion. This makes it impossible to display the laser output as a repetitive oscilloscope pattern and requires that data be taken from a single sweep of the oscilloscope beam. This can be done either with a memory oscilloscope that has a sufficiently fast writing rate or by photographing the interferometer pattern from a standard oscilloscope trace. Photographs have been used in the present study. No room motion is evident during the short (approximately 40 μs)

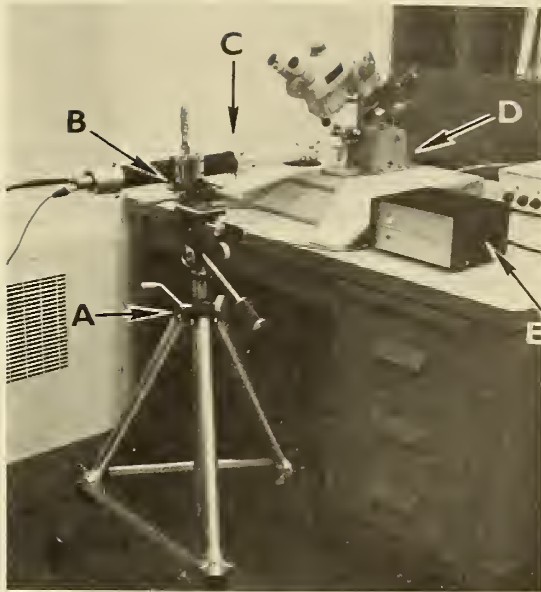

A — HEAVY DUTY TRIPOD WITH STABILIZED BASE
B — X-, Y-, AND Z-AXIS MICROMETER ADJUSTMENTS FOR AIMING THE LASER
C — LASER SYSTEM WITH FOCUSING OPTICS NEAREST THE BONDING MACHINE AND DETECTOR AT THE REAR
D — BONDING MACHINE
E — LASER POWER SUPPLY

Figure 6. Laser system set-up for calibrating ultrasonic bonding tool vibration amplitude.

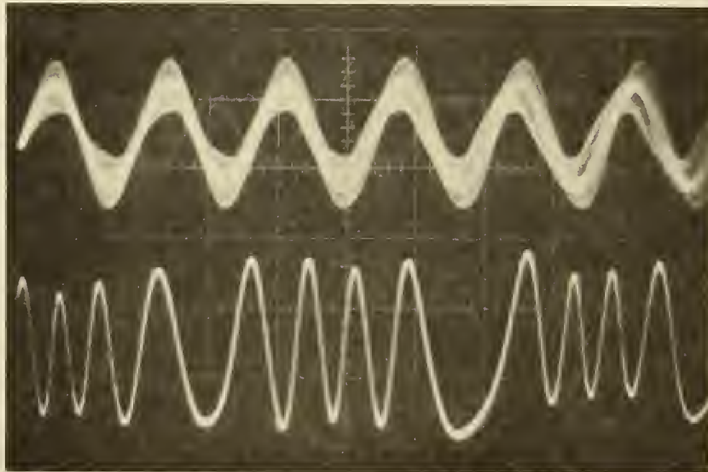

Figure 7. A comparison between the cutput of a microphone and a laser interferometer simultaneously monitoring the same loose bonding tool. (The upper curve is the output of the capacitor microphone and encompasses about five repetitive traces with approximately 5.5 tool motion cycles in each trace. Distortion of the wave shape is obvious. The horizontal scale is approximately 10 μs/div. The lower curve is the laser interferometer output resulting from a single oscilloscope trace covering approximately 1.5 tool motion cycles. The horizontal scale is approximately 2 μs/div.)

sweep period, and the photograph serves as a record that may be preserved for future reference.

In addition to measuring the absolute displacement of bonding tools, the laser has been compared with the capacitor microphone for trouble shooting bonding machines. Since it is not practical to design many different mounting systems to attach the laser rigidly to the variety of bonding machines available, measurements are restricted to a single oscilloscope sweep and thus are not suitable for trouble shooting and diagnostic work. An example is shown in figure 7, a single exposure photograph from a double beam oscilloscope. The upper pattern is a repetitive trace from a capacitor microphone, the lower is a single trace from the laser interferometer. Both instruments were directed toward the same bonding tool on which the set screw had been loosened. The microphone pattern clearly indicates that a problem exists, but the single interferometer trace below does not encompass enough bonding tool vibration cycles to detect the problem. Thus at present the laser is used exclusively for absolute calibration of bonding tool motion. This calibration can then be transferred to more portable measuring devices, such as magnetic pickups and capacitor microphones.

One problem with the small commercial laser employed in the present interferometer is that it is primarily a multimode device. For interferometry, the unit must lase in a single mode. Previously the laser had been tuned to maximum output and then detuned to the TEM_{00} mod. This is a critical adjustment and subject to both amplitude and mode drifting. Even a few percent of a higher mode creates an unacceptable noise level in the detector output. At the suggestion of the manufacturer, special end plates were made to increase the laser cavity length by 1 cm. The mirrors were reinstalled and the laser retuned. This resulted in a laser that operates only in the TEM_{00} mode and therefore makes a better interferometer. (G. G. Harman and A. W. Stallings)

New experiments were undertaken to investigate the process of making aluminum ultrasonic wire bonds and, if possible, to develop measurement methods that may be applicable to in-process bond quality determination. The initial experiment consisted of mixing a local oscillator with the output of a 1/8-in. (0.3-mm) diameter capacitor microphone with a frequency response greater than 200 kHz. The microphone was positioned to pick up sound emitted from the tip of a bonding tool during actual wire bonding. The mixer output was fed into an audio amplifier and from there into a speaker, an oscilloscope, and a tape recorder as shown in the block diagram of figure 8. This apparatus allows the bonding machine operator to listen to an audible beat frequency sound during actual bond formation. Typically, with 0.001-in (25-μm) diameter aluminum wire, an ultrasonic bond is made in about 100 ms which is too short a time for the human ear to distinguish small amplitude or frequency changes. Therefore the audio beat frequency was recorded on magnetic tape and later played back at a

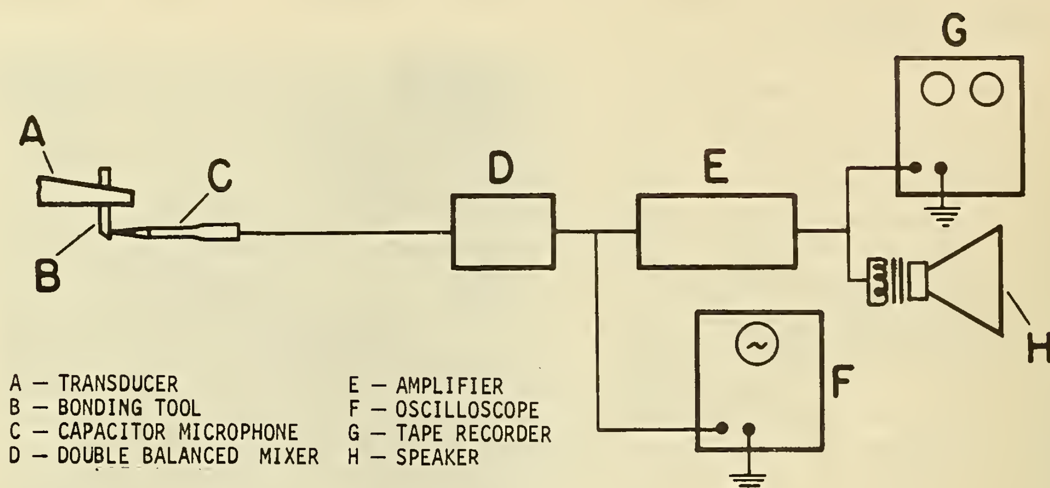

Figure 8. Schematic representation of mixer system for monitoring ultrasonic bond formation.

slower rate so that details of bonding could be both heard and carefully examined on an oscilloscope. Such recordings were made for the fundamental tool vibration frequency through the fourth harmonic, the extreme response limit of the microphone. A brief investigation extending from the fundamental to the fifteenth harmonic was also carried out using the voltage or current from the power supply driving the transducer. At times the bonding machine schedule was modified by reducing the ultrasonic power and increasing the bonding time so that the bonding process could be heard more clearly in real time.

This initial study was made using two ultrasonic power supplies of different manufacture. However, only one bonding machine, one transducer, and one bonding tool extension were used in the tests. Some variation in the results could be expected if the latter two had also been changed. The initial results were dependent on the particular power supply used to drive the transducer. For power supply A there was a few percent decrease in the 60-kHz tool vibration amplitude during bonding, while for power supply B there was a 20 percent increase. These differences are presumably a function of the electronic feedback systems in each power supply as well as the method of transducer drive, which is constant current in one and constant power in the other. As would be expected, differences were observed in the various harmonic relationships during bonding. The second harmonic of both supplies increased in amplitude but in the case of power supply B an unusual frequency warbling was heard during part of each bond. The third harmonic of power supply A was pure tone that increased 5 to 6 dB in amplitude as the tool touched the wire or substrate. There was an additional increase of several decibels during actual bonding.

These large increases in amplitude of the third harmonic which is generated by pressure on the tool are in general agreement with a simple theory of a damped mechanical mass-spring system [2].

The results for both power supplies were a function of the microphone pickup position with respect to the vibrating bonding tool. The largest amplitude changes were obtained with the microphone near the bottom of the tool, close to the wire. The smallest changes were observed with the microphone in front of the transducer horn. Similarly small changes were also observed when the mixer was connected directly to the electrical drive of the transducer.

This experiment was originally intended to be run with a special power-supply-transducer combination in which the transducer is a self-tuning element of the oscillator circuit. Thus as the tool motion is affected by the bonding process both the frequency and the amplitude can be expected to change, producing two measurable variables during bond formation. The power supply and transducer did not arrive during the quarter and thus the initial experiments were performed with a fixed frequency system. (G. G. Harman)

Eight magnetic pickups were assembled and eight bonding machine mounts for either magnetic pickups or capacitor microphones were made at the request of a sponsor. A procedure for using both this equipment and capacitor microphones to tune and trouble shoot ultrasonic wire bonding equipment has been prepared [3].
(G. G. Harman, H. K. Kessler, G. P. Spurlock, and A. W. Stallings)

Additional studies of extraneous machine-induced motions were carried out with the electromagnetic displacement sensor during actual bonding on a second bonding machine. Results were similar to those reported previously (NBS Tech. Note 571, p. 27). A typical oscillogram of the motion between the machine housing, which supports the bonding tool, and the work stage with the motor and all cams operating is shown in figure 9. The indicated motion is in the side-to-side direction. The trace in figure 9a covers the part of the bonding cycle from first search through bonding to loop formation. The upper trace displays the ultrasonic bonding pulse to indicate when the bonding occurs. The lower curve, on the same time scale, shows the various self-induced bonding machine vibrations. Maximum vibration amplitudes about 13 μm peak-to-peak during and immediately after the bond is formed are indicated by fluctuations in the envelope amplitude. As the machine goes into the loop position, a displacement of the entire housing is indicated where the envelope of the oscillogram decreases to about one fifth its initial value. Vibrations with amplitude of 5 μm or more peak-to-peak continue into this portion of the cycle, with several peaks approaching 13 μm.

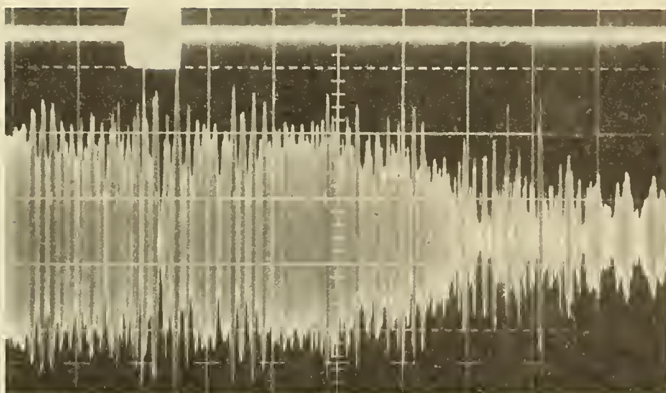

a: First search position through bonding and into loop position.

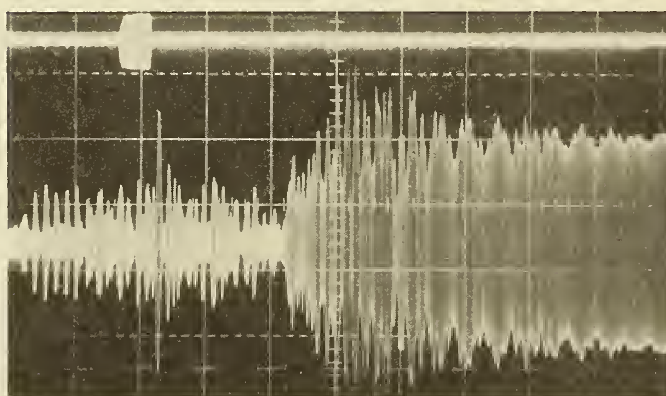

b: Second search position through bonding and wire cutoff to reset position.

Figure 9. Measurement of the self-induced vibrations of a bonding machine. (The upper trace displays the ultrasonic bonding pulse. The lower trace gives the output of the displacement sensor. The vertical scale for the lower trace (displacement) is 2.5 μm/div. The horizontal scale for both traces is 100 ms/div.)

The trace in figure 9b covers the next part of the bonding cycle from second search, through second bonding and wire cutoff, to the starting or reset position. The temporary displacement of the housing which occurred earlier in the cycle continues until wire cutoff, at which time the housing moves back to its original position accompanied by large vibrations with initial amplitudes approaching 13 μm. After this, the vibrations damp out as the machine reaches its starting position and the cam motor stops.

A vibration study was made of each individual cam, including the operating levers, in order to determine in which cam and lever combination the vibration originated. It was found that each cam and lever has its own vibration characteristics, but if all cams and levers are operating, some vibrations are amplified and others are cancelled out.

(H. K. Kessler)

Equipment Improvements — An improved electromagnetic displacement sensor was built for the wire indentation tester previously described (NBS Tech. Note 560, p. 37). As shown in figure 10a, it is shielded both magnetically and electrostatically to prevent pickup from the motor and other moving parts of the tester. The system shown in Figure 10b, is designed to simulate the bonding operation insofar as the wire characteristics are concerned. The wire is indented at regular intervals by a wedge with dimensions similar to those of a bonding tool. A fixed force is applied to the wire each time and the depth of impression is measured by the displacement sensor and recorded. Any irregularities can be readily observed and hence the indentation qualities of the wire assessed.

Modifications were made to the bond-pulling apparatus to allow pulling of bonds at a maximum rate of 77 gf/s (764 mN/s).

(H. K. Kessler and A. W. Stallings)

Bibliography and Critical Review — The first draft of the bibliography on microelectronic wire bonds was completed. The bibliography is a compilation with key words of over 200 published articles, U. S. Government reports, U. S. Patents, standards, and conference talks relevent to wire bonds in three areas: testing, fabrication, and degradation. An attempt was made to make the collection of papers on test and evaluation methods complete while the collection of articles in the areas of fabrication and degradation is meant to be representative. While articles published as early as 1957 are included, the bibliographic search concentrated on the period from 1965 to 1970, inclusive. The selection of papers was generally limited to those that were pertinent to wire bonds where the wire diameter is less than about 50 μm (0.002 in.) and where the wire is bonded by either thermocompressive or ultrasonic means.

Revision of the first draft of the critical survey paper was begun.

(H. A. Schafft and E. C. Cohen)

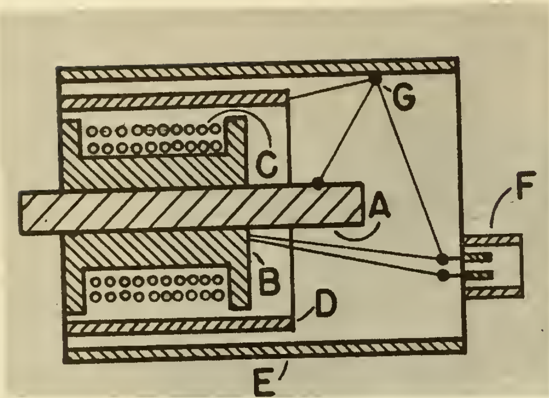

A — LAMINATED MU-METAL CORE
B — COIL FORM
C — COIL
D — MU-METAL SHIELD
E — BRASS SHIELD
F — OUTPUT CONNECTOR
G — GROUND CONNECTION

a: Improved pickup coil for electro-magnetic displacement sensor.

A — LIFTING ARM CAM
B — LIFTING ARM
C — DRIVE MOTOR
D — SENSOR HEIGHT ADJUSTMENT
E — DISPLACEMENT SENSOR, PICKUP COIL
F — ELECTRICAL INPUT CONNECTOR
G — SAPPHIRE ANVIL
H — ELECTRICAL OUTPUT CONNECTOR
I — WIRE FEED CAPILLARY
J — WIRE FEED SPOOL
K — WIRE TAKE-UP SPOOL
L — WIRE FEED HEIGHT ADJUSTMENT
M — DISPLACEMENT SENSOR, DRIVER HEAD
N — LOCATION OF WEIGHT
O — WIRE FEED RATE CONTROL

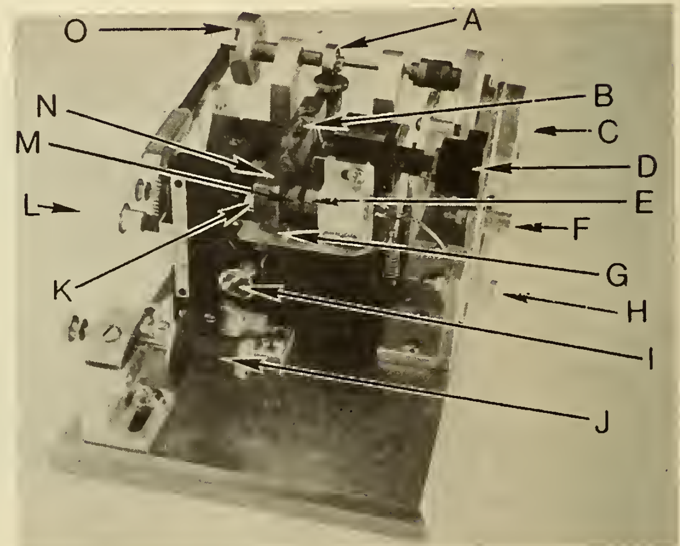

b: Indentation tester.

Figure 10. Improved electromagnetic displacement sensor and wire indentation tester.

Plans: Laser interferometry calibration and other studies of bonding tool motion will continue. Further work on electronic mixing of bonding tool signals with local oscillators will resume after the special power-supply-transducer combination is received. Evaluation of ribbon wire for ultrasonic bonding will resume after the ribbon wire bonder is received following modification by its manufacturer. Work on the wire indentation tester will continue. Experimental and statistical analysis of significant factors in the wire bond pull test will continue. Further assistance will be given to sponsors in connection with problems encountered on device production lines. Preparation of the bibliography and revisions of the first draft of the survey paper will continue.

4.4. PROCESSING FACILITY

Objective: To establish a microelectronic fabrication laboratory with the facilities and procedures necessary for the production of specialized silicon devices for use in research on measurement methods.

Progress: A 10-kW electron beam evaporation system was installed for the deposition of aluminum. A photograph of the system, with the planetary substrate drive (NBS Tech. Note 560, p. 39), is shown in figure 11. This system offers several advantages over the tungsten filament system it replaces because it makes possible very high aluminum deposition rates (in excess of 0.5 μm/min). Since the evaporation rate is high, the contamination of the metal is lower. Experience with *p*-channel, metal-oxide-semiconductor structures revealed that contaminated aluminum was one of the primary contributions to excessive threshold voltages.

(T. F. Leedy, J. Krawczyk, and L. M. Smith)

Figure 11. Electron-beam evaporation system.

A system was built for the purpose of depositing vitreous silicon dioxide films from silane. This process is useful when a silicon dioxide layer must be produced at low temperature. Such oxide films may be used for diffusion masks, for thin film components, or to protect a chip from abrasion. The source

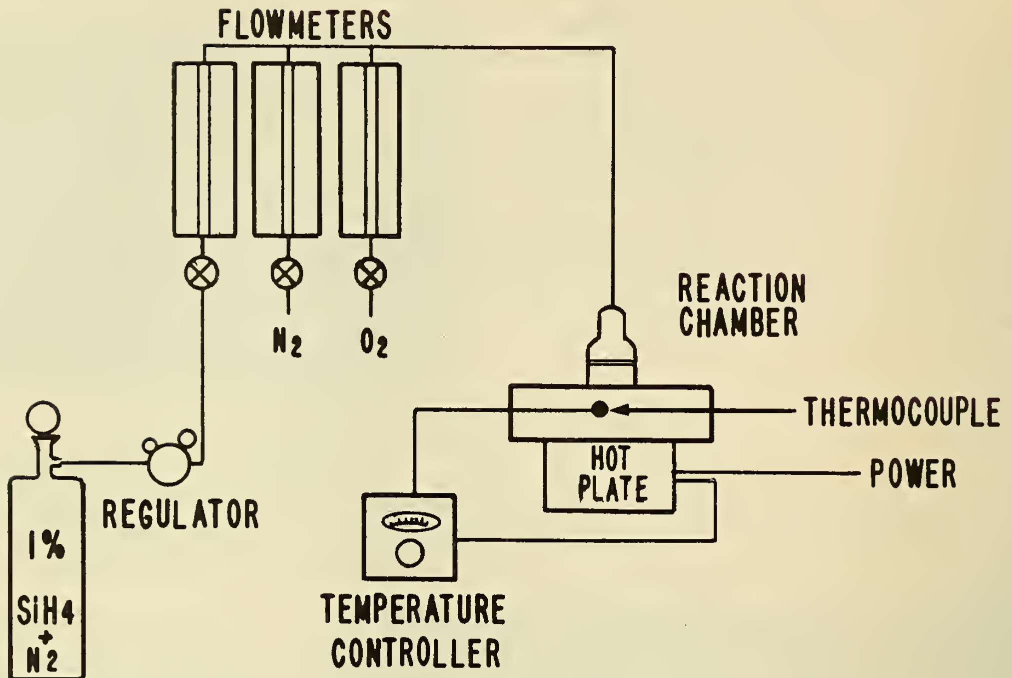

Figure 12. Schematic representation of silicon dioxide vapor deposition system.

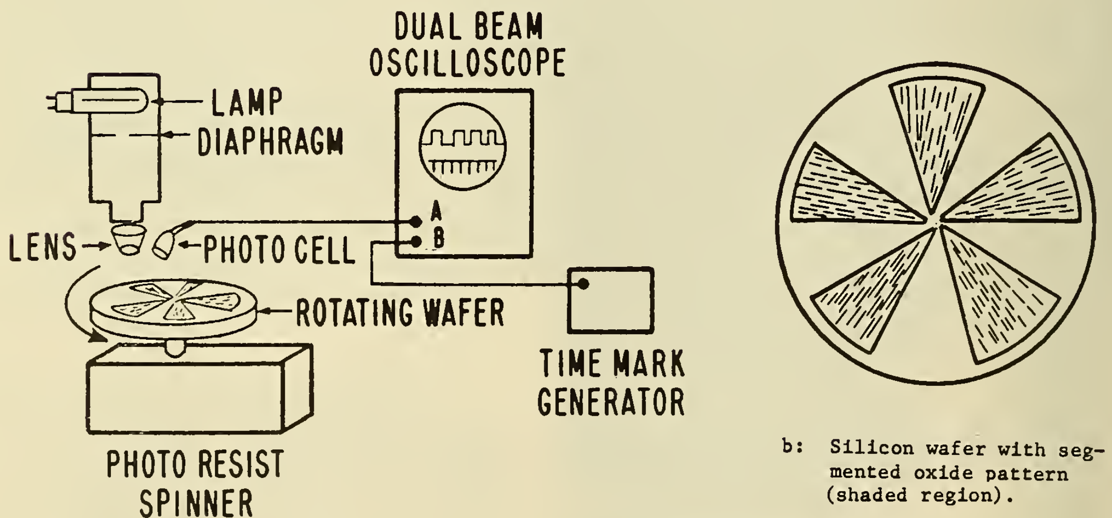

b: Silicon wafer with segmented oxide pattern (shaded region).

a: Schematic representation.

Figure 13. Apparatus for measuring dynamics of photoresist spinners.

material is commercially available high-purity silane. A silicon dioxide deposit is produced by reacting nitrogen-diluted silane with oxygen at temperatures ranging from 200 to 500°C. The system constructed is shown schematically in figure 12. The wafers to be coated are placed on a heated glass plate in the reaction chamber. Since the deposition rate is temperature sensitive the wafer temperature must be held constant to ±1°C [1]. The design of the reaction chamber is critical to the production of uniform films at high deposition rates. Of prime concern are the total flow rate, the geometry of the chamber, and the uniformity of the substrate temperature.

Preliminary infrared analysis of films deposited at 350°C shows the same features as observed for thermally produced oxides with one exception. The absorption peak at 9.2 μm associated with thermally produced oxides was shifted to a higher wavelength (9.7 μm), characteristic of less dense, deposited oxides [2]. The dielectric constant of the deposited oxide measured at 1 MHz was observed to be 4.50, again characteristic of such films, as opposed to 3.85 for the thermally grown films.
(T. F. Leedy, J. Krawczyk, and E. I. Klein)

A simple method was developed for the measurement of the dynamics of photoresist spinners. The final thickness of a photoresist film depends on the angular acceleration of the wafer as well as its terminal angular velocity [3]. To assure that a photoresist spinner will produce films of consistent thickness, the acceleration must be measured and controlled. The angular acceleration is dependent on the torque, the moment of inertia of the rotating components, and other physical parameters of the spinner system.

The measurement apparatus is shown in figure 13. A silicon wafer of the same size that is used in a standard monolithic process is oxidized to appear dark blue in color (oxide approximately 0.13 μm thick). The oxide is etched in a radial pattern as shown in figure 13b. Utilizing the difference in the reflectivity in the pattern, a light source and a photocell sense the passage of the pattern as the wafer rotates on the spinner. The output of the photocell, representing the passage of each segment, is displayed on the oscilloscope. By incorporating an accurate timing pulse into the oscilloscope display, both the acceleration and final velocity can be determined. (T. F. Leedy and J. Krawczyk)

Plans: A three-tube furnace will be installed and made operational to permit the increased diffusion capability presently needed. Additional measurements on thin dielectric films will be started to determine their characteristics more precisely. Study of the techniques to determine spinner dynamics will be continued.

4.5. REFERENCES

4.1. Metallization Evaluation

1. Collins, L. E., Perkins, J. G., and Stroud, P. T., Effect of Ion Bombardment on the Adhesion of Aluminum Films on Glass, *Thin Solid Films* 4, 41-45 (1969).

2. Hamilton, B., and Rawson, H., Fracture of Glass Under a Stationary Ball with Combined Normal and Tangential Loading, *Brit. J. Phys. D: Appl. Phys.* 3, L40-L44 (1970).

3. Weaver, C., and Hill, R. M., Adhesion of Evaporated Aluminum Films, *Phil. Mag.* 3, 1402-1410 (1958).

4.2. Die Attachment Evaluation

1. Daniels, R. G., Thermal Management of Integrated Circuits — Part I. Heat Transfer and Integrated Circuits, *Electro-Technology* 83, No. 1, 22-30 (January, 1969).

4.3. Wire Bond Evaluation

1. Martin, B. D., and Wilson, A. D., An In-Line Laser Interferometer Applied to Ultrasonic Bonder Characterization, 1970 IEEE Ultrasonics Symposium, San Francisco, California, October 21, 1970.

2. Salzer, T., Raytheon Co., Sudbury, Mass., private communication.

3. Harman, G. G., and Kessler, H. K., Application of Capacitor Microphones and Magnetic Pickups to the Tuning and Trouble Shooting of Microelectronic Ultrasonic Bonding Equipment, NBS Tech. Note 573, May, 1971.

4.4. Processing Facility

1. Goldsmith, N., and Kern, W., The Deposition of Vitreous Silicon Dioxide Films from Silane, *RCA Review* 28, 153-165 (1967).

2. Pliskin, W. A., Lehman, J. S., Structural Evaluation of Silicon Oxide Films, *J. Electrochem. Soc.* 112, 1013-1019 (1965).

3. Damon, G. F., The Effect of Whirler Acceleration on the Properties of Photoresist Film, *Proc. Second Kodak Seminar on Microminiaturization*, 34-36 (1966).

☆ U.S. GOVERNMENT PRINTING OFFICE : 1971 481-323/15

5. METHODS OF MEASUREMENT FOR SEMICONDUCTOR DEVICES

5.1. THERMAL PROPERTIES OF DEVICES

Objective: To evaluate and improve electrical measurement techniques for determining the thermal characteristics of semiconductor devices.

Progress: The literature search for methods to measure thermal resistance and transient thermal response of semiconductor devices was continued. Work on the bibliography and review paper was continued, although in a lower priority status. (M. Sigman and F. F. Oettinger)

Work has continued on the preparation of a suitable measurement procedure and data collection format for the preliminary thermal resistance round robin being conducted by JEDEC Committee JC-25 on Power Transistors. The capabilities of on-line measuring equipment available to participants are being determined in order to obtain information to assist in establishing the conditions to be used for the test. (F. F. Oettinger)

A study was conducted to determine what effect variations in device case temperature would have on the voltage at which a hot spot was formed. Measurements of base current, I_B, as a function of collector-emitter voltage, V_{CE}, at constant collector current, I_C, for case temperatures of 25 to 100°C indicated that the voltage level at which the hot spot was formed is nearly independent of the case temperature. Typical curves, shown in figures 14 and 15, indicate that the change in the value of V_{CE} at which the hot spot occurs as the case temperature increased from 25 to 100°C, although small, is greatest under low I_C, high V_{CE} operating conditions. The change under these conditions may be due to the temperature dependence of the avalanche characteristic of the collector-base junction at V_{CE} levels close to the breakdown voltage. Preliminary infrared microradiometer measurements indicated that at the voltage at which the hot spot was formed, the maximum hot-spot temperature increased approximately 75°C when the case temperature was raised from 25 to 100°C. These results suggest that hot-spot formation is governed by the magnitude of a localized temperature increase (which may occur as a result of device geometry, device construction, or junction or bulk anomalies) rather than by the absolute temperature of the chip, but that the maximum temperature in the hot spot is affected by the case or chip temperature. The results appear to be consistent with both the lateral thermal instability model [1] and the previously proposed thermal hysteresis model (NBS Tech. Note 520, pp. 49-52).

To allow study of the thermal inertia of the hot spot during thermal hysteresis, modification of existing equipment was considered. It was found that such modification would compromise its usefulness for the study of thermal resistance and common emitter current gain. The design and fabrication of a second, more flexible measuring system was started. (S. Rubin, G. J. Rogers, and F. F. Oettinger)

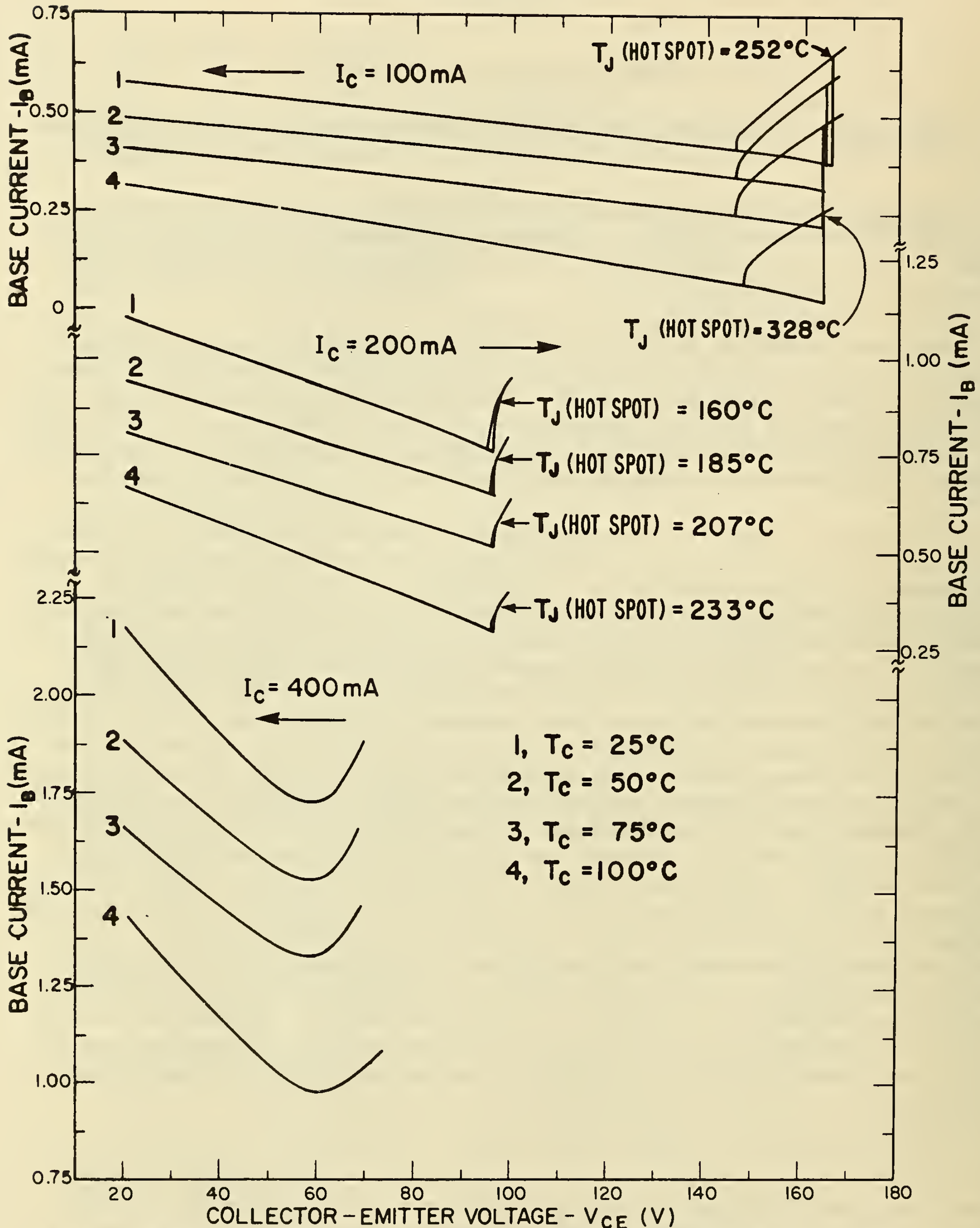

Figure 14. Base current as a function of collector-emitter voltage for a 35-W, triple-diffused, silicon transistor. (The curves were generated for various values of case temperature, T_C, and collector current, I_C, as noted. Since each curve was generated while holding I_C constant, $1/I_B$ is proportional to h_{FE}. The peak junction temperature, T_J, as measured with an infrared microradiometer at the voltage at which the hot-spot was formed is also given for some cases. The hot spots form at the minima of the curves.)

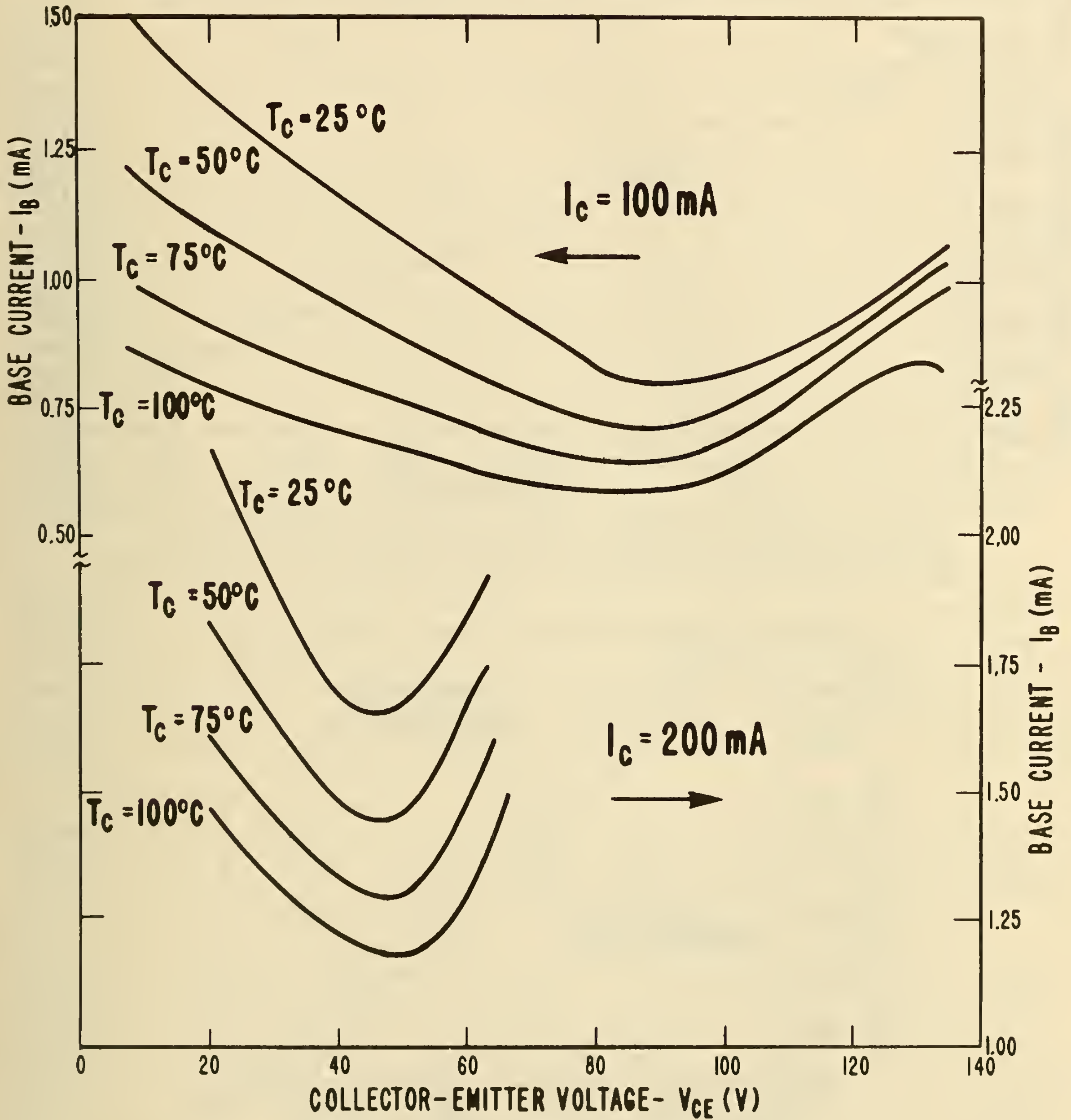

Figure 15. Base current as a function of collector-emitter voltage for a 20-W, triple-diffused, silicon power transistor. (The curves were generated for various values of case temperature, T_C, and collector current, I_C, as noted. Since each curve was generated while holding I_C constant, $1/I_B$ is proportional to h_{FE}. Hot spots form at the minima of the curves.)

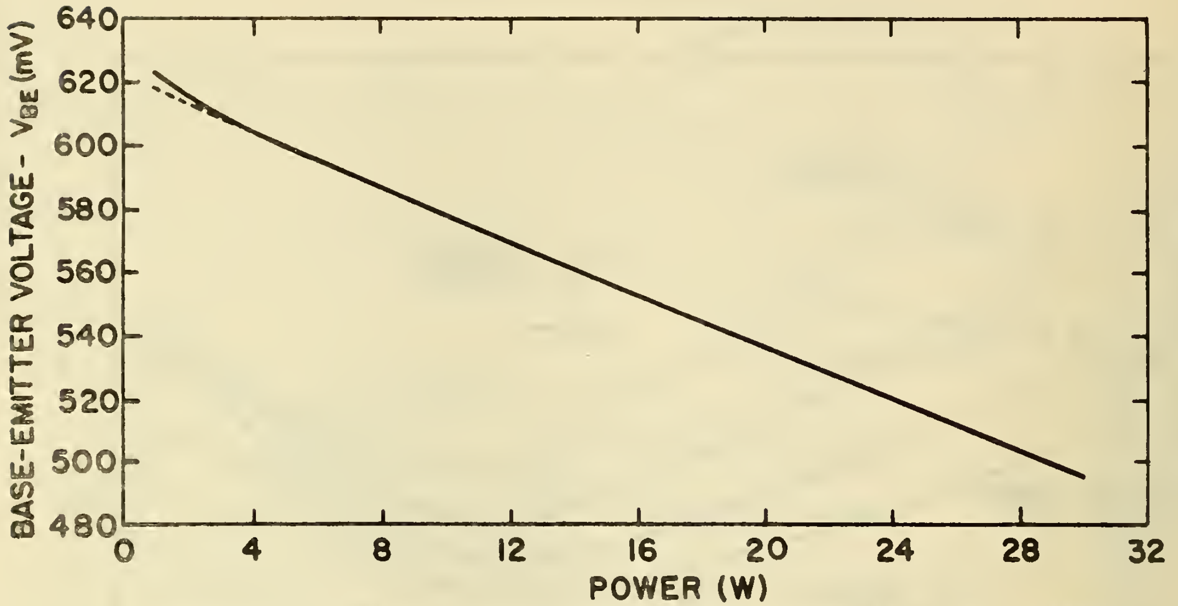

a. Base-emitter voltage as a function of applied power. The base-emitter voltage was measured 12 μs after switching to the measuring base current of 6.5 mA. During the application of power the collector current was 1 A; case temperature was held at 25°C.

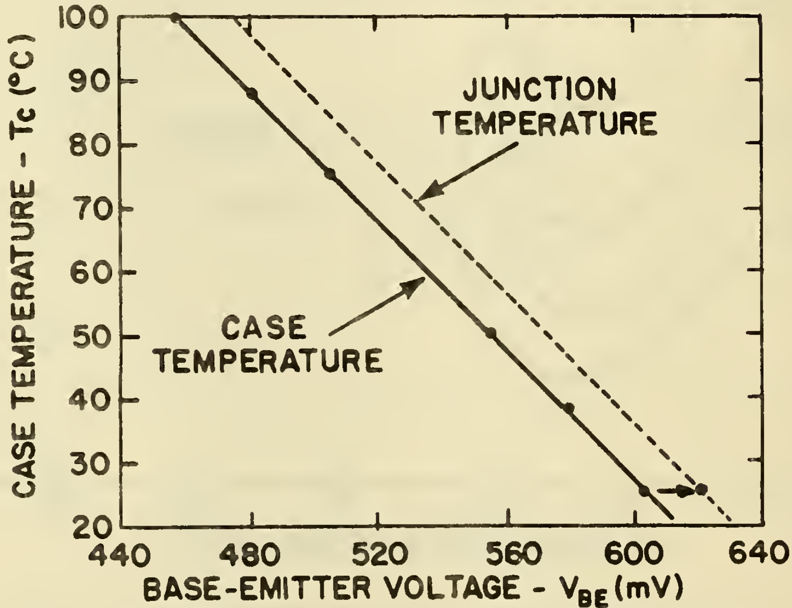

b. Dynamic calibration curve. In this calibration procedure the transistor under test was switched from the operating condition V_{CE} = 4 V, I_C = 1 A to the measuring condition I_B = 6.5 mA. The base-emitter voltage was measured 12 μs after switching to the low level measuring current.

Figure 16. Data used to calculate the thermal resistance of a 35-W, triple-diffused, silicon transistor as a function of applied power.

Electrical measurements of thermal resistance, R_Θ, and common emitter current gain, h_{FE}, as a function of V_{CE} and applied power for I_C up to 200 mA have been reported (NBS Tech. Note 571, pp. 35-42). The base switching circuit and the operational amplifier used to control the collector current were modified to increase the collector current capabilities of the measuring system to 1 A. Typical raw data used to calculate thermal resistance as a function of applied power are shown in figure 16. Base-emitter voltage, V_{BE}, measured for a metering current of 6.5 mA, 12 μs after the end of the power pulse, is plotted as a function of power in figure 16a (solid line). Below 4 W, (I_C = 1 A, V_{CE} = 4 V), an increase in non-thermal switching effects, probably due to the decrease in h_{FE} as V_{CE} is decreased, causes the V_{BE} curve to become nonlinear. Although the non-thermal effects become less significant if the delay in measuring the temperature sensitive parameter is increased from 12 to 17 μs, the additional cooling of the junction that occurs during the longer delay time may result in falsely low values for R_Θ. If the non-thermal switching effects were not present, V_{BE} at low power levels would have the values represented by the dashed line in figure 16a provided the linear relationship between power and junction temperature, T_J, extends to zero power dissipation where V_{BE} = 621 mV.

The dynamic calibration, shown in figure 16b, was carried out by switching from a low-power condition (V_{CE} = 4 V, I_C = 1 A) to the measuring condition (V_{CE} open, I_B = 6.5 mA) for case temperature, T_C, from 25 to 100°C. Under these conditions T_J is somewhat greater than T_C. The junction temperature may be found by displacing the case temperature line to the right so that the extrapolated value of V_{BE} for zero power dissipation (621 mV) corresponds with 25°C as shown by the arrow in figure 16b.

The thermal resistance, R_Θ, can be found from the slopes of the linear plots in figure 16a and b: $R_\Theta = (\Delta T_C/\Delta V_{BE})(\Delta V_{BE}/\Delta W)$. For the example shown in figure 16, R_Θ = (0.514°C/mV) (4.23 mV/W) = 2.2°C/W. In figure 17, h_{FE} for this device, a 35-W, triple-diffused, silicon transistor, is plotted together with R_Θ as computed above. The data indicate that there is no decrease in h_{FE} as V_{CE} is increased so apparently no appreciable current constriction occurs. It should be noted that if R_Θ had been calculated from the non-linear portion of the V_{BE} against power curve there would have been an apparent increase in R_Θ with decreasing power. It has been shown previously (NBS Tech. Note 571, pp. 35-42) that for this type of device structure the actual chip thermal resistance does not increase with decreasing power. (S. Rubin and F. F. Oettinger)

In some cases, an increase in R_Θ is observed as T_C is increased. An experiment was conducted to determine if this increase in R_Θ can be related to the increase in the thermal resistivity of the silicon chip with temperature. Measurements were made on a 35-W, epitaxial diffused, silicon transistor with a silicon-chip-to-total-device thermal resistance ratio of approximately 1 to 3. The thermal resistance measured for

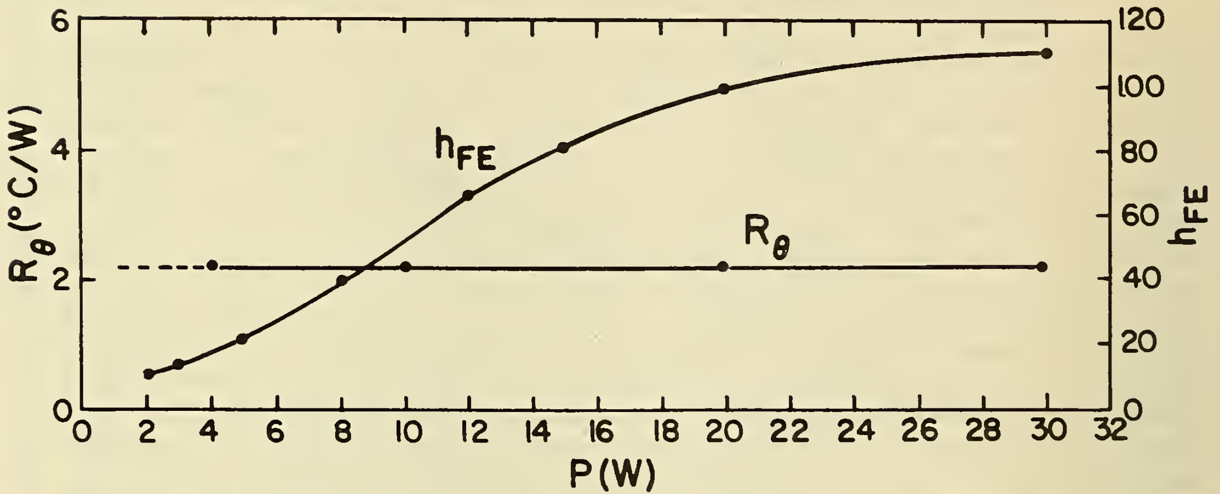

Figure 17. Common-emitter current gain, h_{FE}, and thermal resistance, R_Θ, of a 35-W, triple-diffused, silicon transistor as a function of applied power, P. (Case temperature was held at 25°C. The thermal resistance was calculated from the data shown in Figure 16.)

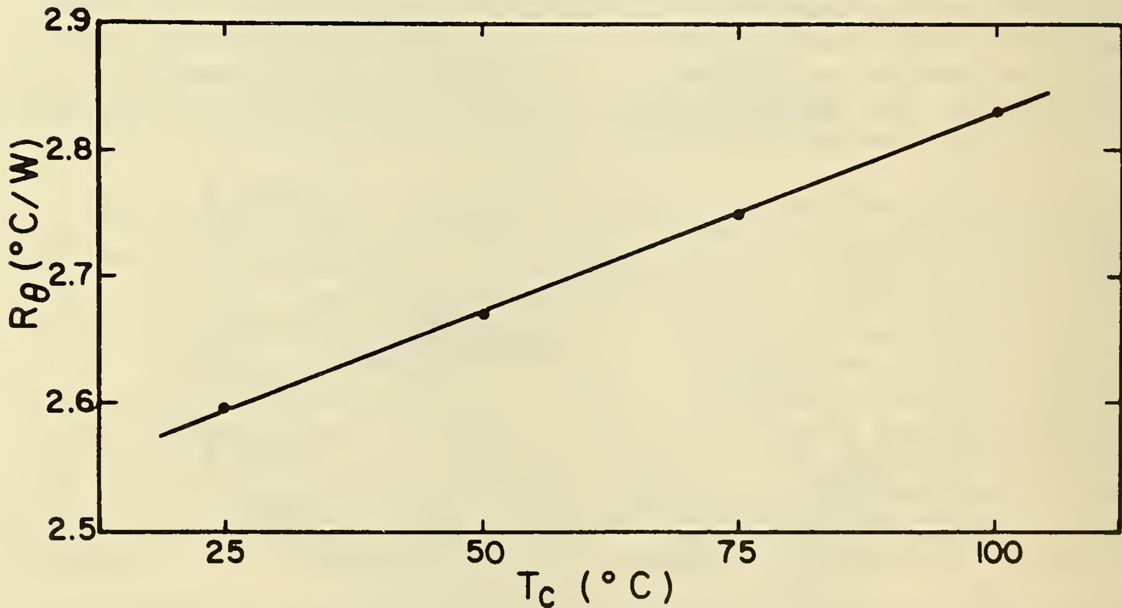

Figure 18. Thermal resistance, R_Θ, as a function of case temperature, T_C, for a 35-W, epitaxial-diffused, silicon transistor. (During the application of power the collector current was 500 mA. The base-emitter voltage, from which the thermal resistance was derived, was measured 12 μs after switching to a low level measuring current.)

I_C = 500 mA and for V_{CE} from 1 to 16 V at case temperatures ranging from 25 to 100°C is plotted as a function of T_C in figure 18. In these experiments dynamic calibration curves were run beginning at case temperatures of 25, 50, 75, and 100°C so that the effect of the temperature dependence of R_Θ on the relationship between T_C and T_J under calibration conditions (power dissipation of 4 W) could be neglected.

The measured increase in R_Θ for an increase in T_C of from 25 to 75°C was 9 percent while the calculated increase in R_Θ expected because of the increase in the thermal resistivity of the silicon chip over the same temperature range was approximately 12 percent. The calculation was based on thermal conductivity data reported by Shanks [2] and the assumption that about one third of the temperature drop from junction to mounting surface is due to the thermal resistance of the silicon chip [3]. Although it has been known that the thermal resistivity of silicon is temperature dependent, most experimenters have not considered this effect. The results of this study indicate that, for devices with a significant chip-to-total-device thermal resistance ratio, the effect of the variation of the thermal resistivity of silicon with temperature should be considered when determining the test conditions for R_Θ measurements. For such devices, either R_Θ should be measured at maximum rated junction temperature or a derating factor should be generated to allow for the increase in thermal resistance of silicon with temperature.

(S. Rubin, G. G. Rogers, and F. F. Oettinger)

Plans: The literature search, work on the bibliography and writing of the first draft of the review paper on thermal resistance and transient thermal response measurements will continue.

The measurement procedure and data collection format for the Committee JC-25 preliminary thermal resistance round robin will be established. The measurements will be made on TO-66 and TO-3 encased power transistors. It is expected that R_Θ will be measured after operation of transistors in high-current, low voltage conditions: I_C = 0.5 to 1 A and V_{CE} = 10 to 20 V.

Design and fabrication of the more flexible system for measuring R_Θ and h_{FE} will continue. Various studies pertaining to hot-spot formation and thermal hysteresis can be carried out with the new system.

Measurement of R_Θ and h_{FE} as a function of power for various collector current levels will continue. Infrared microradiometer and thermographic phosphor measurements will then be made on the same devices to investigate relationships which may exist between the peak temperature and the electrically-measured temperature.

Objective: To evaluate the utility of thermographic techniques for detection of hot spots and measurement of temperature distribution in semiconductor devices.

Progress: A 50-μm diameter fiber optic probe and scanning eyepiece for the photometric microscope was received but had to be returned for correction of defects in the mechanical drive. The spatial resolution of the 50-μm and 150-μm diameter probes were compared by scanning a black-white boundary on the 1.0 pattern of a Microcopy Resolution Test Chart* with each and recording the output of the photometer. The results are shown in figure 19.

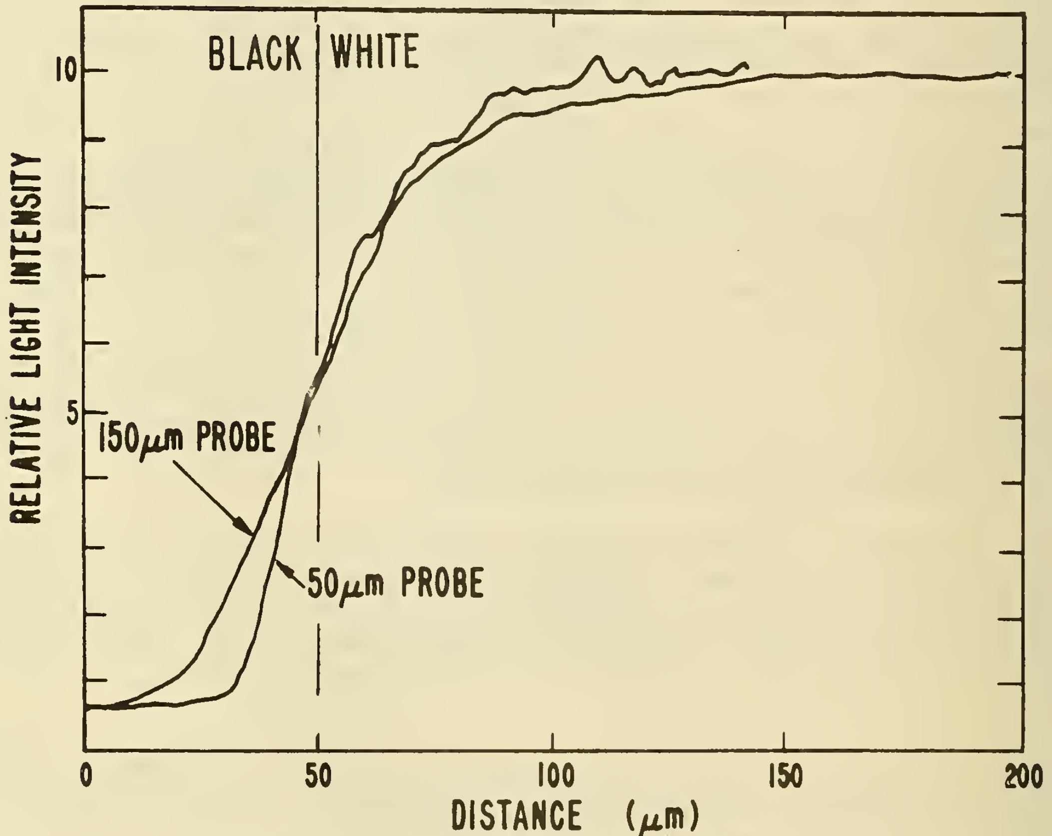

Figure 19. Spatial resolution of fiber optic probes compared by scanning a black-white boundary on a Microcopy Resolution Test Chart and recording the changes in photometer output. (The 7 to 1 reduction in light output from the 50-μm probe was compensated by increasing the amplification of the photometer and recorder.)

---

* Available as SRM-1010a from the Office of Standard Reference Materials, National Bureau of Standards, Washington, D. C. 20234. The 1.0 pattern consists of 0.5-mm wide alternate black and white stripes.

A preliminary evaluation of the performance of the infrared microscope indicated that temperatures can be measured with a precision of ±1°C. If emissivity is known, the accuracy is about ±2°C for temperatures above 45°C; the accuracy is poorer between 25 and 45°C. The infrared microscope was used to make temperature profile and spot temperature measurements on several power transistors whose thermal properties had previously been checked electrically. Further work was interrupted by a malfunction which prevented zeroing the output of the microscope.
(G. J. Rogers, F. F. Oettinger, and L. R. Williams)

Plans: Temperature calibration of the thermographic phosphors will be completed. When the IR microscope is again available, comparison of the relative capabilities of the IR microscope and thermographic phosphors will be resumed.

5.3. MICROWAVE DEVICE MEASUREMENTS

Objective: To study the problems and uncertainties associated with the measurement of microwave devices, and to improve the techniques of these measurements.

Progress: The audio i-f portion of the X-band mixer diode measurement system (NBS Tech. Note 571, pp. 43-45) was built and tested. It uses an automatic switch and an oscilloscope to compare a precision d-c reference voltage with the peaks of the 1-kHz square wave used as the i-f signal. This i-f voltage is used to calculate mixer conversion loss. The need for better shielding became apparent when measurements closer than ±0.5 mV were attempted. Bypassing the load and bias circuits and using a 50-Ω coaxial load to terminate the mixer for both a-c and d-c allowed measurements to better than ±50 μV. This represents a precision of ±0.1 percent for a 6-dB conversion loss mixer output voltage of about 50 mV peak-to-peak across a normal 400-Ω i-f load, using a 1-dB peak-to-trough modulation which is equivalent to a single-frequency r-f signal of about -28 dBm. The precision was limited by the presence of a non-random, non-sinusoidal noise whose origin has not been determined. Based upon the resolution obtained with the reference voltage trace, another order-of-magnitude improvement in precision would be possible if this noise were eliminated (leaving only the random oscilloscope and system noise).

Mixer conversion loss is based upon available, rather than delivered, output power, and its determination thus requires a knowledge of the source immittance which is predominately resistive at audio i-f's. Equations were developed which enable the mixer i-f resistance and open-circuit i-f voltage to be calculated from measurements of normal mixer i-f voltages across two different finite values of load resistance. This obviates the use of an external i-f signal source as with a bridge measurement. The closer the two resistance values are to each other, the

less is the dependency on mixer linearity and the less is the effect of circuit reactances, but the precision is lower.

Preliminary measurements, which were limited by available equipment to a ±0.5 mV precision for load voltages of about 20 to 90 mV, seemed to indicate that the mixer i-f resistance as calculated from these equations is independent of load resistance over the range from 100 Ω (equal to the d-c load) to 100 kΩ (essentially an open circuit for the mixer). Extensive proof of this independence, however, using higher precision and a variety of diodes, is required before complete mixer output linearity can be assumed for the measurement.

To obtain i-f resistance and open-circuit i-f voltage without calculation, a measurement technique was developed to enable the mixer i-f resistance to be read directly from a calibrated precision decade resistance box. Setting the i-f load to this value then enables half the open-circuit mixer i-f voltage to be measured directly. A search of the literature revealed that this method was invented in the nineteenth century by Sir Henry Mance to measure battery resistance [1-3]. This method is related to a method invented by Kelvin [3] for measuring galvanometer resistance and appears to have been lost to later generations. It seems well worth reviving, since the apparently unrecognized ability of the method to enable a source immittance to be measured with only small load variations makes it potentially valuable for non-linear and high-power devices, where the load immittance must be maintained close to a nominal value at all times. It appears that the method can be applied to microwave and other high-frequency sources by using a hybrid junction, which is the high-frequency analog of the Wheatstone bridge whose theory forms the basis for Mance's method.

In further study of the r-f portion of the X-band system the local oscillator power occasionally drifted in amplitude to a small but objectionable extent, even though the klystron is frequency stabilized by being phase-locked to a crystal-controlled oscillator. Stable local oscillator power is of fundamental importance to all mixer measurements, but is particularly important to modulation-type conversion loss measurements, where the r-f test signal is proportional to the power of the local oscillator from which it is derived. In order to improve the local oscillator amplitude stability, a preliminary, experimental version of a feedback loop (leveler) was built and tested. The circuit contained a diode detector, an operational amplifier, and the PIN modulator that had been previously connected for amplitude modulation. The leveler successfully maintained the power available to the mixer independent of klystron power variations (over the several decibel range of excess power available) to within the discernible limits of measurement (less than ±50 μV). Power to the mixer was set by means of the operational amplifier offset voltage control, thus obviating a d-c reference supply. A clean, stable modulation was obtained by applying a low-level square wave to the non-inverting op-amp input terminal. (J. M. Kenney)

Plans: The r-f portion of the circuit will be rebuilt to permit leveling during actual mixer measurements. This will require extensive and difficult alterations of the r-f circuit because of the need to isolate the monitoring detector from power reflected by the mixer and to relocate the precision attenuator used to measure the degree of modulation to a point following the feedback loop. The modulator which is now connected by a switch and a coaxial line will be moved to the main wave guide line to avoid loss and leakage, a harmonic-absorption pad will be added to minimize the reflection, back to the mixer, of local oscillator and signal harmonics generated by the mixer, and several other components will be relocated to improve circuit performance.

Following this, the audio i-f circuit will be redesigned, to incorporate Mance's method for measuring mixer i-f resistance, and rebuilt on a shielded chassis. Mance's method, and its application to low and high frequency measurements, will be reported upon at a later date after some experience with it is obtained.

5.4. CARRIER TRANSPORT IN JUNCTION DEVICES

Objective: To improve methods of measurement for charge carrier transport and related properties of junction semiconductor devices.

Progress: On the recommendation of sponsors, visits were made to discuss methods for making transistor delay time measurements with the participants in previous comparative tests of the measurement: the Air Force Weapons Laboratory, Sandia Laboratories, and Bendix Research Corporation. Similar discussions were held with personnel from the Boeing Aircraft Company (a contractor of a sponsor) and from the NBS Electromagnetics Division.

Laboratory work was focused on assembly, initial testing, and adjustment of the Sandia-type delay-time bridge [1] constructed in this laboratory. Measurements on the bridge were made between 3 and 30 MHz. It was found that the signal generator to be used with the bridge must be carefully shielded and have a power output of 0.2 W or greater and that connections between the bridge, signal generator and radio receiver (used for null detection) must also be well shielded. Lack of adequate shielding shows up, in the extreme case, by nulls not being obtained, or in less severe cases, by a strong frequency dependence of the delay zero-set value. The transistorized current amplifier which interfaces between the transistor under test and the null detector in the original Sandia version of the bridge was duplicated with minor modifications to increase its stability.*

---

* The amplifier was modified and constructed by D. J. Brenner of the NBS Measurement Engineering Division.

A preliminary analysis of the Sandia bridge* showed that if the line stretchers (which are used as the adjustable delay elements) are terminated — as they are — in their characteristic impedance of 50 Ω at the attenuator-phase splitter ends, the delay time read from the line stretchers should be independent of any mismatch between the other ends of the line stretchers and the transistor being measured. This is an important result since it is known that transistor impedance varies with frequency, bias conditions, and type. It was also stated that electrical isolation of 40 dB between the "test" and "reference" line stretchers is required to achieve a negligible (< 1 percent) measurement error. A measurement at 10 MHz yielded isolation of 57 dB on the bridge constructed in this laboratory.

As a continuation of the literature survey and evaluation of existing techniques for application to the project goals, literature citations demonstrating that an analysis of transistor noise spectra should yield values of base transit time are being compiled. References on the problem of making electrical probe measurements on transistors prior to metalization are also being collected. (D. E. Sawyer)

Plans: Delay-time measurement and probing techniques will continue to be discussed with appropriate workers in the field. The compiling of literature citations on these two topics, and on the application of noise spectrum analysis to the determination of device internal processes, will continue.

Pertinent measurement data will be obtained on the Sandia delay-time bridge including interchannel isolation frequency, the ratio (which should be unity, ideally) of "test" to "reference" line delay for null as a function of frequency, and initial delay. Construction of the socket and biasing arrangement for the vector voltmeter will be completed. It is planned that work on both the Sandia bridge and the vector voltmeter system will be completed at about the same time so that initial transistor delay time measurements can be made on both instruments to provide comparative data.

5.5. SILICON NUCLEAR RADIATION DETECTORS

Objective: To conduct a program of research, development, and device evaluation in the field of silicon nuclear radiation detectors with emphasis on the improvement of detector technology, and to provide consultation and specialized device fabrication services to the sponsor.

* Carried out by D. Ellerbruch of the NBS Electromagnetics Division.

Progress: Pre-flight bench-testing of lithium-drifted silicon radiation detectors continued. Initial experiments were conducted in the ambient exposure test program to determine the effects of hazardous ambients on the performance characteristics of lithium-drifted and surface-barrier silicon detectors. Eight lithium-drifted silicon detectors were acquired for radiation damage experiments.

Testing and Evaluation — Commercial lithium-drifted, surface-barrier and diffused-junction silicon radiation detectors were given extensive bench tests as part of a continuing program of detector evaluation and acceptance for the sponsor.* An unusually high percentage of the large area (850 mm^2) devices failed to meet performance specifications when operated under high-vacuum conditions. Several ultra-thin (2 to 5 μm) surface-barrier detectors were evaluated for use in a particle identification telescope. While the general performance of these detectors was found to be satisfactory, their excessive capacitances resulted in a large electrical noise contribution by the charge-sensitive preamplifiers used. In addition a few diffused-junction detectors were examined. In general these devices performed poorly, due primarily to bad electrical contacts and thick particle entrance windows.

(Y. M. Liu and J. M. Morrison)

Radiation Damage — A literature search of radiation effects in lithium-drifted silicon detectors and related subjects was completed. In preparation for the next phase of the radiation damage study, eight lithium-drifted silicon detectors were purchased from a commercial source.

(Y. M. Liu and B. H. Audet)

Ambient Exposure Tests — Silicon radiation detectors on future spacecraft, notably Pioneer F, are expected to be subjected to certain harmful gases and vapors, both before and after launch, which may have a detrimental effect on their performance. Prior to launch such solvents as methyl alcohol and certain commercial leak detector fluids used to check pressure and vacuum seals are used in and around the spacecraft. After launch, the attitude in space of the satellite will be periodically adjusted by hydrazine thrusters, which are expected to leave a low pressure shroud of ammonia gas around the spacecraft. The pressure of this shroud is not known at this time.

A glass vacuum system was assembled to provide an appropriate environment for determining the effect of such gases and vapors on detector performance. Initial experiments revealed problems with excessive outgassing within the system. The glass system was disassembled, and construction of a new system, utilizing a stainless steel test chamber and

---

* Detailed data resulting from these tests have been transmitted to the sponsor.

stainless steel, greaseless ultra-high vacuum valves was begun. The new completely bakeable system is expected to solve the outgassing problem.
(E. I. Klein and B. H. Audet)

Plans: Exhaustive pre-flight bench-testing of detectors will continue as required by the sponsor. The radiation damage study in lithium-drifted silicon detectors will begin. The new ambient exposure test system will be completed and tested.

5.6. REFERENCES

5.1. Thermal Properties of Devices

1. Scarlett, R. M., and Shockley, W., Secondary Breakdown and Hot Spots in Power Transistors, *IEEE International Convention Record* 11, Part 3, 3-13 (1963).

2. Shanks, H. R., Maycock, P. D., Sidles, P. H., and Danielson, G. C., Thermal Conductivity of Silicon from 300 to 1400°K, *Phys. Rev.* 130, 1743-1748 (1963).

3. Daniels, R. G., Thermal Management of Integrated Circuits, Part I, Heat Transfer and Integrated Circuits, *Electro-Technology* 83, No. 1, 22-30 (January, 1969).

5.3. Microwave Device Measurements

1. Price, W. A., *A Treatise on the Measurement of Electrical Resistance,* Clarendon Press, Oxford, 1895, pp. 153-155, 192-196 (Appendix V).

2. Roller, F. W., *Electric and Magnetic Measurements and Measuring Instruments,* McGraw Publishing Co., N. Y., 1907, pp. 146-148.

3. Northrup, E. F., *Methods of Measuring Electrical Resistance,* McGraw Hill Book Co., N. Y., 1912, pp. 218-219 (Art. 1106). Also: Kelvin's Method, *ibid,* p. 235 (Art. 1117).

5.4. Carrier Transport in Junction Devices

1. Sullivan, W. H., A New Technique for the Direct Measurement of Minority Carrier Base Transit Time in the Junction Transistor, Sandia Laboratories Report SC-DR-69-419, September, 1969. Available from the National Technical Information Service, Springfield, Va. 22151.

Appendix A

JOINT PROGRAM STAFF

Coordinator: J. C. French
Consultant: C. P. Marsden

Semiconductor Characterization Section
(301) 921-3625

Dr. W. M. Bullis, Chief

A. J. Baroody, Jr.
D. L. Blackburn
F. H. Brewer
Mrs. E. C. Cohen*
M. Cosman
Dr. J. R. Ehrstein
G. G. Harman
Mrs. R. E. Joel+
H. K. Kessler
Mrs. K. O. Leedy
Miss C. A. Main
R. L. Mattis
Dr. W. E. Phillips
Mrs. T. A. Schultz+
Miss D. R. Ricks
H. A. Schafft
A. W. Stallings
G. N. Stenbakken
W. R. Thurber

Semiconductor Processing Section
(301) 921-3541

Dr. A. H. Sher, Acting Chief×

B. H. Audet
H. A. Briscoe
W. K. Croll
Mrs. S. A. Davis+
H. E. Dyson*
W. J. Keery
E. I. Klein
J. Krawczyk
T. F. Leedy
Y. M. Liu
Miss J. M. Morrison
J. Oroshnik
L. M. Smith
G. P. Spurlock

Electron Devices Section
(301) 921-3622

J. C. French, Chief

Mrs. C. F. Bolton+
Mrs. R. Y. Cowan
Miss B. S. Hope+
R. L. Gladhill
J. M. Kenney
F. F. Oettinger
M. K. Phillips
R. C. Powell*
G. J. Rogers
S. Rubin
D. E. Sawyer
M. Sigman
L. R. Williams

---

* Part Time
\+ Secretary
× Dr. J. A. Coleman is on temporary assignment to Office of Associate Director for Programs.

COMMITTEE ACTIVITIES

ASTM Committee F-1 on Electronics
- A. J. Baroody, Lifetime Section
- C. F. Bolton, Committee Assistant Secretary
- W. M. Bullis, Editor, Subcommittee 4, Semiconductor Crystals; Leaks, Resistivity, Mobility, Dielectrics, and Compound Semiconductors Sections
- J. A. Coleman, Secretary, Subcommittee 5, Semiconductor Processing Materials
- J. R. Ehrstein, Resistivity, Epitaxial Resistivity, and Epitaxial Thickness Sections
- J. C. French, Committee Editor
- T. F. Leedy, Photoresist Section
- C. P. Marsden, Committee Secretary
- R. L. Mattis, Lifetime Section
- J. Oroshnik, Thick Films and Photomasking Sections; Chairman, Thin Films Section
- W. E. Phillips, Crystal Perfection, Encapsulation, Thin Films, and Thick Films Sections; Chairman, Lifetime Section
- A. H. Sher, Germanium Section
- M. Sigman, Editor, Subcommittee 5, Semiconductor Processing Materials
- W. R. Thurber, Mobility, Germanium, and Impurities in Semiconductors Sections

Electronic Industries Association; Solid State Products Division, Joint Electron Device Engineering Council (JEDEC):
- J. M. Kenney, Microwave Diode Measurements, Committee JC-21 on UHF and Microwave Diodes
- F. F. Oettinger, Chairman, Task Group on Thermal Considerations for Microelectronic Devices, Committee JC-11 on Mechanical Standardization; Technical Advisor, Thermal Resistance Measurements, Committees JC-22 on Thyristors, JC-20 on Signal Diodes, and JC-25 on Power Transistors
- R. C. Powell, Microwave Diode Measurements, Committee JC-21 on UHF and Microwave Diodes; Task Group on Transistor Scattering Parameter Measurement Standards, Committee JC-24 on Low Power Transistors
- S. Rubin, Chairman, Council Task Group on Galvanomagnetic Devices
- H. A. Schafft, Technical Advisor, Second Breakdown and Related Specifications, Committee JC-25 on Power Transistors

IEEE Electron Devices Group:
- J. C. French, Standards Committee
- J. M. Kenney, Chairman, Standards Committee Task Force on Microwave Solid State Devices II (Mixer and Video Detector Diodes)

H. A. Schafft, Chairman, Standards Committee Task Force on Second Breakdown Measurement Standards

IEEE Nuclear Science Group:

J. A. Coleman; Administrative Committee; Nuclear Instruments and Detectors Committee; Editorial Board, *Transactions on Nuclear Science;* Chairman, 1970 Nuclear Science Symposium

A. H. Sher, Technical Program Committee, 1970 Nuclear Science Symposium

IEEE Magnetics Group

S. Rubin, Chairman, Galvanomagnetic Standards Subcommittee

Society of Automotive Engineers

J. C. French, Subcommittee A-2N on Radiation Hardness and Nuclear Survivability

IEC TC47, Semiconductor Devices and Integrated Circuits:

S. Rubin, Technical Expert, Galvanomagnetic Devices; U. S. Specialist for Working Group 5 on Hall Devices and Magnetoresistive Devices

NMAB ad hoc Committee on Materials and Processes for Electronic Devices:

W. M. Bullis

Appendix C

SOLID-STATE TECHNOLOGY & FABRICATION SERVICES

Technical services in areas of competence are provided to other NBS activities and other government agencies as they are requested. Usually these are short-term, specialized services that cannot be obtained through normal commercial channels. Such services provided during the last quarter are listed below and indicate the kinds of technology available to the program.

1. Radiation detectors — (B. H. Audet)
   Design and development of fabrication procedures were begun for a 52 element lithium-drifted silicon detector array to be used as an electron scattering hodoscope by the Electronuclear Physics Section.

2. Sectioning and plating — (H. A. Briscoe)
   Transistors were sectioned, polished, and stained to reveal cross-sectional geometries, small piece parts were gold or nickel plated, and silver films were vacuum evaporated on several types of plastics for other groups in the Electronic Technology Division.

3. Quartz and glass fabrication — (E. I. Klein)
   A quartz closure for a vacuum system for growing barium crystals was fabricated for the Physical Chemistry Division.

4. Ultrasonic fabrication — (J. Krawczyk)
   Four pieces of piezoelectric ceramic were ultrasonically machined for the Naval Ship Research and Development Center.

Appendix D

JOINT PROGRAM PUBLICATIONS

Prior Reports:

A review of the early work leading to this Program is given in Bullis, W. M., Measurement Methods for the Semiconductor Device Industry— A Review of NBS Activity, NBS Tech. Note 511, December, 1969.

Quarterly reports covering the period since July 1, 1968, have been issued under the title Methods of Measurement for Semiconductor Materials, Process Control, and Devices.

Quarter Ending	NBS Tech. Note	Date Issued	DDC Accession No.
September 30, 1968	472	December, 1968	AD 681330
December 31, 1968	475	February, 1969	AD 683808
March 31, 1969	488	July, 1969	AD 692232
June 30, 1969	495	September, 1969	AD 695820
September 30, 1969	520	March, 1970	AD 702833
December 31, 1969	527	May, 1970	AD 710906
March 31, 1970	555	September, 1970	AD 718534
June 30, 1970	560	November, 1970	AD 719976
September 30, 1970	571	April, 1971	

Current Publications:

Bullis, W. M., Measurement Methods for Microcircuits, *Space Simulation,* J. C. Richmond, Ed., NBS Spec. Publ. 336, October, 1970, pp. 449-455.

Silicon Device Processing, C. P. Marsden, Ed., NBS Spec. Publ. 337, November, 1970.

Sher, A. H., Carrier Trapping in Ge(Li) Detectors, *IEEE Trans. Nucl. Sci.* NS-18, No. 1, 175-183 (February, 1971).

Liu, Y. M., and Coleman, J. A., Electron Radiation Damage Effects in Silicon Surface-Barrier Detectors, *IEEE Trans. Nucl. Sci.* NS-18, No. 1, 192-199 (February, 1971).

Rubin, S., and Oettinger, F. F., Thermal Hysteresis and its Possible Effect on Restriction of the Hot-Spot Free Operating Range of Some Power Transistors, to be published in *IEEE Trans. Electron Devices,* June, 1971.

Harman, G. G., and Kessler, H. K., Application of Capacitor Microphones and Magnetic Packups to the Tuning and Trouble Shooting of Microelectronic Ultrasonic Bonding Equipment, NBS Tech. Note 573, May, 1971.

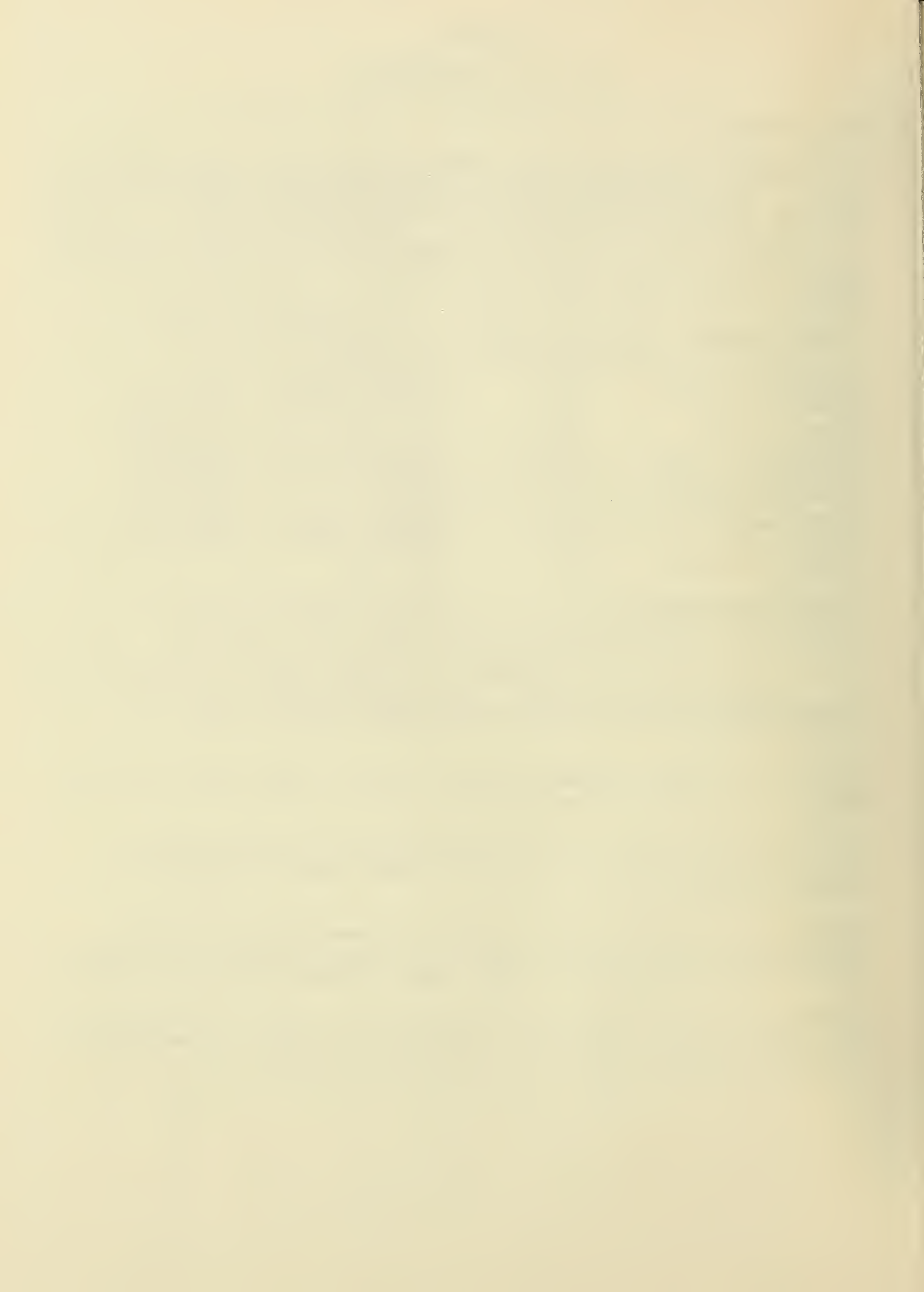

FORM NBS-114A (1-71)

U.S. DEPT. OF COMM. BIBLIOGRAPHIC DATA SHEET	1. PUBLICATION OR REPORT NO. NBS-TN-592	2. Gov't Accession No.	3. Recipient's Accession No.

4. TITLE AND SUBTITLE
Methods of Measurement for Semiconductor Materials, Process Control, and Devices. Quarterly Report, October 1 to December 31, 1970

5. Publication Date August 1971

6. Performing Organization Code

7. AUTHOR(S) W. Murray Bullis, Editor

8. Performing Organization

9. PERFORMING ORGANIZATION NAME AND ADDRESS

NATIONAL BUREAU OF STANDARDS
DEPARTMENT OF COMMERCE
WASHINGTON, D.C. 20234

10. Project/Task/Work Unit No. See Item 15

11. Contract/Grant No. See Item 12

12. Sponsoring Organization Name and Address Natl. Bureau of Standards, DASA (EA071-801), Navy Strategic Systems Project Office, NAD, Crane, Indiana (PO-1-0030 and PO-1-0041), Navy Electronics System Command (PO-1-1057), AEC, and NASA (S-70003-G and H-76553A)

13. Type of Report & Period Covered Interim Oct. 1 to Dec. 31, 1970

14. Sponsoring Agency Code

15. SUPPLEMENTARY NOTES 4251120, 4251123, 4251126, 4251449, 4252114, 4252119, 4252128, 4252534, 4254111, 4254112, 4254115, 4254429, 4259425, 4259522, 4259533.

16. ABSTRACT (A 200-word or less factual summary of most significant information. If document includes a significant bibliography or literature survey, mention it here.)

This quarterly progress report, tenth of a series, describes NBS activities directed toward the development of methods of measurement for semiconductor materials, process control, and devices. Significant accomplishments during this reporting period include successful application of the surface photovoltage technique, a non-contacting method, to the measurement of carrier diffusion length in silicon epitaxial layers and development of a novel, but simple, method for measurement of acceleration and terminal angular velocity of a photoresist spinner. Work is continuing on measurement of resistivity, carrier lifetime, and electrical inhomogeneities in semiconductor crystals; specification of germanium for gamma-ray detectors; evaluation of wire bonds, metallization adhesion, and die attachment; measurement of thermal properties of semiconductor devices, transit-time and related carrier transport properties in junction devices, and electrical properties of microwave devices; and characterization of silicon nuclear radiation detectors. Supplementary data concerning staff, standards committee activities, technical services, and publications are included as appendixes.

Key Words (cont.): measurement; microelectronics; microwave devices; nuclear radiation detectors; probe techniques (a-c); resistivity; semiconductor devices; semiconductor materials; semiconductor process control; silicon; thermal resistance; thermographic measurements; ultrasonic bonder; wire bonds.

17. KEY WORDS (Alphabetical order, separated by semicolons) Alpha-particle detectors; aluminum wire; base transit time; carrier lifetime; die attachment; electrical properties; epitaxial silicon; gamma-ray detectors; germanium; gold-doped silicon; metallization; methods of

18. AVAILABILITY STATEMENT	19. SECURITY CLASS (THIS REPORT)	21. NO. OF PAGES
[XX] UNLIMITED.	UNCLASSIFIED	72
[ ] FOR OFFICIAL DISTRIBUTION. DO NOT RELEASE TO NTIS.	20. SECURITY CLASS (THIS PAGE) UNCLASSIFIED	22. Price 50 cents

NBS TECHNICAL PUBLICATIONS

PERIODICALS

JOURNAL OF RESEARCH reports National Bureau of Standards research and development in physics, mathematics, chemistry, and engineering. Comprehensive scientific papers give complete details of the work, including laboratory data, experimental procedures, and theoretical and mathematical analyses. Illustrated with photographs, drawings, and charts.

Published in three sections, available separately:

- **Physics and Chemistry**

Papers of interest primarily to scientists working in these fields. This section covers a broad range of physical and chemical research, with major emphasis on standards of physical measurement, fundamental constants, and properties of matter. Issued six times a year. Annual subscription: Domestic, $9.50; foreign, $11.75*.

- **Mathematical Sciences**

Studies and compilations designed mainly for the mathematician and theoretical physicist. Topics in mathematical statistics, theory of experiment design, numerical analysis, theoretical physics and chemistry, logical design and programming of computers and computer systems. Short numerical tables. Issued quarterly. Annual subscription: Domestic, $5.00; foreign, $6.25*.

- **Engineering and Instrumentation**

Reporting results of interest chiefly to the engineer and the applied scientist. This section includes many of the new developments in instrumentation resulting from the Bureau's work in physical measurement, data processing, and development of test methods. It will also cover some of the work in acoustics, applied mechanics, building research, and cryogenic engineering. Issued quarterly. Annual subscription: Domestic, $5.00; foreign, $6.25*.

TECHNICAL NEWS BULLETIN

The best single source of information concerning the Bureau's research, developmental, cooperative and publication activities, this monthly publication is designed for the industry-oriented individual whose daily work involves intimate contact with science and technology—*for engineers, chemists, physicists, research managers, product-development managers, and company executives.* Annual subscription: Domestic, $3.00; foreign, $4.00*.

* Difference in price is due to extra cost of foreign mailing.

NONPERIODICALS

Applied Mathematics Series. Mathematical tables, manuals, and studies.

Building Science Series. Research results, test methods, and performance criteria of building materials, components, systems, and structures.

Handbooks. Recommended codes of engineering and industrial practice (including safety codes) developed in cooperation with interested industries, professional organizations, and regulatory bodies.

Special Publications. Proceedings of NBS conferences, bibliographies, annual reports, wall charts, pamphlets, etc.

Monographs. Major contributions to the technical literature on various subjects related to the Bureau's scientific and technical activities.

National Standard Reference Data Series. NSRDS provides quantitative data on the physical and chemical properties of materials, compiled from the world's literature and critically evaluated.

Product Standards. Provide requirements for sizes, types, quality and methods for testing various industrial products. These standards are developed cooperatively with interested Government and industry groups and provide the basis for common understanding of product characteristics for both buyers and sellers. Their use is voluntary.

Technical Notes. This series consists of communications and reports (covering both other agency and NBS-sponsored work) of limited or transitory interest.

Federal Information Processing Standards Publications. This series is the official publication within the Federal Government for information on standards adopted and promulgated under the Public Law 89–306, and Bureau of the Budget Circular A–86 entitled, Standardization of Data Elements and Codes in Data Systems.

Consumer Information Series. Practical information, based on NBS research and experience, covering areas of interest to the consumer. Easily understandable language and illustrations provide useful background knowledge for shopping in today's technological marketplace.

NBS Special Publication 305, Supplement 1, Publications of the NBS, 1968-1969. When ordering, include Catalog No. C13.10:305. Price $4.50; foreign, $5.75.

Order NBS publications from: Superintendent of Documents
Government Printing Office
Washington, D.C. 20402

U.S. DEPARTMENT OF COMMERCE
National Bureau of Standards
Washington, O.C. 20234

OFFICIAL BUSINESS

Penalty for Private Use, $300

POSTAGE ANO FEES PAIO
U.S. OEPARTMENT OF COMMERCE